arXiv:1403.2252v2 [cond-mat.str-el] 5 Jun 2014

Frustrated spin-$\frac{1}{2}$ J_1–J_2 isotropic XY model on the honeycomb lattice

R. F. Bishop,[1] P. H. Y. Li,[1] and C. E. Campbell[2]

[1] *School of Physics and Astronomy, Schuster Building, The University of Manchester, Manchester, M13 9PL, UK*

[2] *School of Physics and Astronomy, University of Minnesota, 116 Church Street SE, Minneapolis, Minnesota 55455, USA*

We study the zero-temperature ground-state (GS) phase diagram of a spin-half J_1–J_2 XY model on the honeycomb lattice with nearest-neighbor exchange coupling $J_1 > 0$ and frustrating next-nearest-neighbor exchange coupling $J_2 \equiv \kappa J_1 > 0$, where both bonds are of the isotropic XY type, using the coupled cluster method. Results are presented for the GS energy per spin, magnetic order parameter, and staggered dimer valence-bond crystalline (SDVBC) susceptibility, for values of the frustration parameter in the range $0 \leq \kappa \leq 1$. In this range we find phases exhibiting, respectively, Néel xy planar [N(p)], Néel z-aligned [N(z)], SDVBC, and Néel-II xy planar [N-II(p)] orderings. The Néel-II states, which break the lattice rotational symmetry, are ones in which the spins of nearest-neighbor pairs along one of the three equivalent honeycomb directions are parallel, while those in the other two directions are antiparallel. The N(p) state, which is stable for the classical version of the model in the range $0 \leq \kappa \leq \frac{1}{6}$, is found to form the GS phase out to a first quantum critical point at $\kappa_{c_1} = 0.216(5)$, beyond which the stable GS phase has N(z) order over the range $\kappa_{c_1} < \kappa < \kappa_{c_2} = 0.355(5)$. For values $\kappa > \kappa_{c_2}$ we find a strong competition to form the GS phase between states with N-II(p) and SDVBC forms of order. Our best estimate, however, is that the stable GS phase over the range $\kappa_{c_2} < \kappa < \kappa_{c_3} \approx 0.52(3)$ is a mixed state with both SDVBC and N-II(p) forms of order; and for values $\kappa > \kappa_{c_3}$ is the N-II(p) state, which is stable at the classical level only at the highly degenerate point $\kappa = \frac{1}{2}$. Over the range $0 \leq \kappa \leq 1$ we find no evidence for any of the spiral phases that are present classically for all values $\kappa > \frac{1}{6}$, nor for any quantum spin-liquid state.

PACS numbers: 75.10.Jm, 05.30.Rt, 75.30.Kz, 75.40.Cx

I. INTRODUCTION

In recent years many theoretical studies have been devoted to various frustrated quantum spin models on the two-dimensional (2D) honeycomb lattice, using several different quantum many-body techniques.[1–15] Particular attention has focused on the spin-$\frac{1}{2}$ J_1–J_2 model in which nearest-neighbor (NN) pairs of spins interact via an isotropic Heisenberg interaction with exchange coupling parameter J_1, and next-nearest-neighbor (NNN) pairs interact via a similar isotropic Heisenberg interaction with exchange coupling parameter J_2. When the NN interaction is antiferromagnetic in nature (i.e., $J_1 > 0$), a corresponding antiferromagnetic NNN interaction (i.e., $J_2 > 0$) acts to frustrate the Néel order that is preferred by the NN bonds acting by themselves. The extended spin-$\frac{1}{2}$ J_1–J_2–J_3 model, in which the additional next-next-nearest-neighbor (NNNN) Heisenberg bonds of exchange coupling strength J_3 are included, has also been studied on the honeycomb lattice. Both spin-$\frac{1}{2}$ models have rich ground-state (GS) zero-temperature ($T = 0$) phase diagrams and, indeed the nature of the ground state is still not fully resolved beyond all doubt in various parts of the phase diagrams. The J_1–J_2–J_3 model in particular even exhibits a diverse array of ordered GS phases in the classical case, which corresponds to the limit $s \to \infty$ of the spin quantum number s of the spins residing on the honeycomb lattice sites.

In view of the uncertainty that sill remains over the $T = 0$ GS phase diagram of the spin-$\frac{1}{2}$ J_1–J_2 Heisenberg model on the honeycomb lattice, it is of great interest to examine closely related models. One such model is the isotropic frustrated J_1–J_2 XY model on the same honeycomb lattice. Whereas the isotropic J_1–J_2 Heisenberg model has the Hamiltonian,

$$\mathcal{H}_{\rm H} = J_1 \sum_{\langle i,j \rangle} \mathbf{s}_i \cdot \mathbf{s}_j + J_2 \sum_{\langle\langle i,k \rangle\rangle} \mathbf{s}_i \cdot \mathbf{s}_k \,, \qquad (1)$$

where index i runs over all honeycomb lattice sites, indices j and k run respectively over all NN and NNN sites to i, counting each bond once only, and $\mathbf{s}_i = (s_i^x, s_i^y, s_i^z)$ is the spin operator (corresponding to a spin quantum number s) on site i, the corresponding isotropic J_1–J_2 XY model has the Hamiltonian,

$$\mathcal{H}_{XY} = J_1 \sum_{\langle i,j \rangle} (s_i^x s_j^x + s_i^y s_j^y) + J_2 \sum_{\langle\langle i,k \rangle\rangle} (s_i^x s_k^x + s_i^y s_k^y) \,. \qquad (2)$$

The two models of Eqs. (1) and (2) on the honeycomb lattice share exactly the same $T = 0$ GS phase diagram in the classical ($s \to \infty$) limit,[1,2] which makes it particularly interesting to compare their corresponding phase diagrams for the extreme quantum limiting case, $s = \frac{1}{2}$. Even at the classical level the two models on the honeycomb lattice share the interesting feature that for values of the frustration parameter $J_2/J_1 \equiv \kappa > \frac{1}{6}$ the GS phase has an infinite degeneracy,[1–3] since in this regime the wave vector $\mathbf{Q}$ of the non-collinear spiral states that

form the stable GS phase can take any value over a specific closed contour in the Brillouin zone, as we discuss more fully in Sec. II.

One knows that novel quantum phases often emerge from such classical models that exhibit an infinitely degenerate family of GS phases in some region of phase space. Typically one then finds that quantum fluctuations lift this (accidental) GS degeneracy, either wholly or partially, by the *order by disorder* mechanism,[16,17] to favor either just one or several members of the classical family as the quantum GS phase. Indeed, for the present models it has been shown[3] that spin-wave fluctuations at leading order, $O(1/s)$, lift the accidental degeneracy in favor of specific wave vectors, thus leading to spiral order by disorder. Nevertheless, it is well known that quantum fluctuations have the general tendency to favor collinear ordering over noncollinear ordering, and one may thus anticipate that for the spin-$\frac{1}{2}$ models in particular the quantum fluctuations present should actually melt the spiral order for a wide range of values of the frustration parameter, κ. One such collinear state, which is among the infinitely degenerate family of ground states at the classical critical point $\kappa = \frac{1}{2}$, is the so-called Néel-II state, in which all NN bonds along one of the three equivalent honeycomb directions are ferromagnetic (i.e., with spins parallel), while those along the other two directions are antiferromagnetic (i.e., with spins antiparallel). This is precisely the state favored by the above-mentioned spiral order by disorder mechanism at the classical critical point $\kappa = \frac{1}{2}$.

Naturally, quantum fluctuations in the extreme $s = \frac{1}{2}$ quantum limit can also be expected to destroy completely the magnetic order in any (collinear or non-collinear) quasiclassical state in various regions of the $T = 0$ GS phase space, i.e., for various regions of the frustration parameter κ. Indeed, such magnetically disordered regions have been observed in a large number of theoretical calculations of the spin-$\frac{1}{2}$ isotropic J_1–J_2 Heisenberg model on the honeycomb lattice, which involve valence-bond crystalline (VBC) phases with either plaquette or dimer ordering.

For example, in a recent calculation[15] by the present authors, using the coupled cluster method (CCM) carried out to very high orders of approximation, the $T = 0$ GS phase diagram of the spin-$\frac{1}{2}$ isotropic J_1–J_2 Heisenberg model on a honeycomb lattice was studied for the case $J_1 > 0$ in the range $0 \leq \kappa \leq 1$ for the frustration parameter. Four phases were found, which exhibited, respectively, Néel, 6-spin plaquette, staggered dimer, and Néel-II orderings, with corresponding quantum critical points (QCPs) at $\kappa_{c_1} = 0.207 \pm 0.003$, $\kappa_{c_2} = 0.385 \pm 0.010$, and $\kappa_{c_3} \approx 0.65 \pm 0.05$. The two transitions at κ_{c_1} [between states with Néel and plaquette valence-bond crystalline (PVBC) order] and κ_{c_3} [between states with staggered dimer valence-bond crystalline (SDVBC) and Néel-II order] were found to be most likely of continuous second-order (and hence deconfined) type, while that at κ_{c_2} (between the two VBC states) was found to be most likely of direct first-order type. The competition between SDVBC and Néel-II orderings was found to be particularly finely balanced, and consequently the QCP at κ_{c_3} has the largest associated uncertainty. Although broadly similar results have been reported using other theoretical method,[2–14] differences still remain and a complete consensus has not yet been reached for the full $T = 0$ GS phase diagram for the spin-$\frac{1}{2}$ Hamiltonian of Eq. (1) on the infinite honeycomb lattice.

Nevertheless, since the CCM has proven itself to give very accurate results for the GS phases and the associated QCPs for a very wide range of other spin-lattice models on 2D lattices (see, e.g., Refs. 7, 18–38, and references cited therein), it now seems an opportune time to apply it also to the closely related spin-$\frac{1}{2}$ isotropic XY model, whose Hamiltonian is given by Eq. (2), in order to compare its $T = 0$ GS phase diagram with our previous results[15] for the spin-$\frac{1}{2}$ Heisenberg model of Eq. (1). This has become particularly timely in view of recent intriguing results[39] for the isotropic XY model, using the density matrix renormalization group (DMRG), which showed a stable GS phase in a relatively narrow region of the frustration parameter κ, immediately beyond the QCP below which Néel antiferromagnetic (AFM) collinear magnetic order occurs in the xy plane, in which Néel AFM order now occurs with the spins aligned along the z axis. This is particularly surprising in view of the total absence in the XY model of any Ising-like terms involving $s_k^z s_l^z$ between spins on any pairs of sites k and l. The spin-$\frac{1}{2}$ isotropic XY model on the honeycomb lattice had also been studied earlier[40] in the context of an equivalent model of spinless hard-core bosons on the honeycomb lattice at half-filling with NN and NNN hopping terms and zero off-site interactions, using the exact diagonalization (ED) of relatively small lattice clusters. This work suggested the existence of a particular quantum spin-liquid (QSL) GS phase in a similar regime of phase space for the parameter κ.

One motivation for the later DMRG study[39] was to examine much larger finite lattice clusters than are feasible for ED studies, in order to investigate whether the QSL GS phase might have been an artefact of the small clusters studied, which would not survive in the thermodynamic limit, $N \to \infty$, where N is the number of lattice sites. Indeed, the DMRG study[39] found no evidence for any QSL phases in the XY model. By contrast, another very recent variational Monte (VMC) study[41] of the isotropic XY model, which employed a variational QSL wave function of a particular type (based on a decomposition of the bosonic particles into pairs of spin-$\frac{1}{2}$ fermions, and including a long-range Jastrow factor plus a Gutzwiller projection to enforce single bosonic occupancy) found that such QSL states are energetically favored in the intermediate frustration regime.

In view of these conflicting results for the spin-$\frac{1}{2}$ isotropic XY model of Eq. (2) on the honeycomb lattice, it seems worthwhile to apply another method to the model. Since the CCM has provided a consistent and ac-

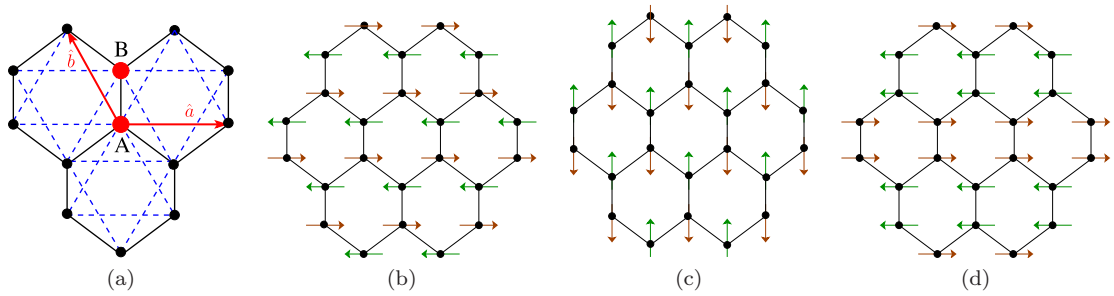

FIG. 1. (Color online) The J_1–J_2 XY model on the honeycomb lattice with $J_1 > 0$ and $J_2 > 0$, showing (a) the bonds ($J_1 \equiv$ —— ; $J_2 \equiv$ – – –), the two sites (●) A and B of the unit cell, and the Bravais lattice vectors $\hat{a}$ and $\hat{b}$; (b) the Néel planar, N(p), state; (c) the Néel z-aligned, N(z), state; and (d) the Néel-II planar, N-II(p), state. For the three states shown the arrows represent the directions of the spins located on lattice sites •.

curate description for the closely related spin-$\frac{1}{2}$ isotropic Heisenberg model of Eq. (1), we now use it again here. In Sec. II we first describe the model itself in more detail, including its classical counterpart, before reviewing the basic ingredients of the CCM itself in Sec. III as it is applied to general spin-lattice problems. The results are then presented in Sec. IV, and we conclude with a summary and discussion in Sec. V.

II. THE MODEL

In this paper we consider the Hamiltonian of Eq. (2) on the honeycomb lattice for the case $s = \frac{1}{2}$. We are interested in the frustrated regime where $J_1 > 0$ and $J_2 \equiv \kappa J_1 > 0$. The lattice and exchange bonds are illustrated in Fig. 1(a). Henceforth we put $J_1 \equiv 1$ to set the energy scale. The honeycomb lattice is a bipartite lattice, and the two sites A and B of the unit cell are also shown in Fig. 1(a), together with the two Bravais lattice vectors $\hat{a} = (1, 0)$ and $\hat{b} = (-\frac{1}{2}, \frac{\sqrt{3}}{2})$, specified in terms of x and y coordinates in the lattice plane. The honeycomb lattice divides into two triangular sublattices $\mathcal{A}$ and $\mathcal{B}$, such that A $\in \mathcal{A}$ and B $\in \mathcal{B}$. We label the sites of the triangular Bravais lattice (i.e., $\mathcal{A}$) as $\mathbf{R}_i = m\hat{a}+n\hat{b} = (m-\frac{1}{2}n, \frac{\sqrt{3}}{2}n)$, and consider the two sites (A and B) in the unit cell to have the same value of $\mathbf{R}_i$.

The Wigner-Seitz unit cell is thus the parallelogram formed by the lattice vectors $\hat{a}$ and $\hat{b}$, although it may equivalently, and often more conveniently, be centered on a point of sixfold rotational symmetry (i.e., at a center of any basic hexagon of the lattice), in which case the unit cell is then bounded by the sides of the hexagon. The first Brillouin zone is then itself a hexagon that is rotated by 90° with respect to the hexagonal Wigner-Seitz cell. A rotation in the plane by 180° around the center of the hexagonal Wigner-Seitz cell (i.e., a 2D inversion) has the effect of interchanging the two sublattices, $\mathcal{A} \to \mathcal{B}$.

We first summarize the results for the classical counterpart of the model, which pertain to both the Heisenberg and XY models of Eqs. (1) and (2) respectively. The most general state with coplanar order in the $x_s y_s$ spin-coordinate plane can be described by a spiral wave with wave vector $\mathbf{Q}$, together with an angle θ that relates to the relative orientations of the two spins in the same unit cell, both described by the same Bravais lattice vector $\mathbf{R}_i$. Thus, we have

$$\mathbf{s}_i^{\mathcal{A}} = s[\cos(\mathbf{Q}\cdot\mathbf{R}_i)\hat{x}_s + \sin(\mathbf{Q}\cdot\mathbf{R}_i)\hat{y}_s]\,; \quad i \in \mathcal{A}\,, \tag{3}$$

for sites i on the sublattice $\mathcal{A}$, and

$$\mathbf{s}_i^{\mathcal{B}} = -s[\cos(\mathbf{Q}\cdot\mathbf{R}_i+\theta)\hat{x}_s + \sin(\mathbf{Q}\cdot\mathbf{R}_i+\theta)\hat{y}_s]\,; \quad i \in \mathcal{B}\,, \tag{4}$$

for sites i on the sublattice $\mathcal{B}$, where $\hat{x}_s$ and $\hat{y}_s$ are orthogonal unit vectors in the $x_s y_s$ spin-coordinate plane, the normal direction to which is the z_s axis, shown as the upward spin direction in Fig. 1(c). The notation of Eqs. (3) and (4) is chosen such that the angle between NN spins on the two sublattices with the same Bravais lattice vectors $\mathbf{R}_i$ is $\theta + \pi$, and hence such that the state with Néel planar [N(p)] order shown in Fig. 1(b) is described by $\mathbf{Q} = \mathbf{\Gamma} \equiv (0, 0)$ and $\theta = 0$.

In this general coplanar spiral state described by Eqs. (3) and (4), the classical GS energy per spin is readily seen to be given by

$$\begin{aligned}\frac{E_{\rm cl}}{N} =& -\frac{1}{2}J_1 s^2[\cos\theta + \cos(\theta - Q_b) + \cos(\theta - Q_a - Q_b)] \\ &+ J_2 s^2[\cos Q_a + \cos Q_b + \cos(Q_a + Q_b)]\,,\end{aligned} \tag{5}$$

where $Q_a \equiv \mathbf{Q}\cdot\hat{a}$ and $Q_b \equiv \mathbf{Q}\cdot\hat{b}$. Clearly Q_a and Q_b are only uniquely defined modulo 2π since, by definition, the addition of arbitrary multiples of 2π to either (or both) quantity simply translates us from the first Brillouin zone to another. Minimization of Eq. (5) with respect to the three parameters Q_a, Q_b and θ then yields the classical GS phase diagram. One finds that for small values of the frustration parameter in the range $0 < \kappa < \frac{1}{6}$ the lowest-energy state is unique (up to rotations in the spin $x_s y_s$ plane), with collinear N(p) AFM ordering and an energy

per spin given by

$$\frac{E_{\rm cl}^{\rm N(p)}}{N} = \frac{3}{2}s^2(-1+2\kappa). \quad (6)$$

with $J_1 \equiv 1$. Conversely, for $\kappa > \frac{1}{6}$, the lowest-energy state is infinitely degenerate, with a wave vector that is specified only by the single relation,

$$\cos Q_a + \cos Q_b + \cos(Q_a + Q_b) = \frac{1}{2}\Big[\Big(\frac{1}{2\kappa}\Big)^2 - 3)\Big]. \quad (7)$$

Thus, for $\kappa > \frac{1}{6}$, the classically degenerate solutions form closed contours in the reciprocal $\mathbf{Q}$-vector space. For each point (Q_a, Q_b) on these contours the phase angle θ is uniquely specified by the relations,

$$\sin\theta = 2\kappa[\sin Q_b + \sin(Q_a + Q_b)]\,, \quad (8)$$

$$\cos\theta = 2\kappa[1 + \cos Q_b + \cos(Q_a + Q_b)]\,. \quad (9)$$

The GS energy per spin for these degenerate spiral phases is given by

$$\frac{E_{\rm cl}^{\rm spiral}}{N} = -\frac{1}{2}s^2\Big(\frac{1}{4\kappa} + 3\kappa\Big)\,, \quad (10)$$

with $J_1 \equiv 1$. By comparison of Eqs. (6) and (10) it is clear that there is a classical continuous second-order transition at $\kappa_{\rm cl} = \frac{1}{6}$ between GS phases with N(p) order for $\kappa < \kappa_{\rm cl}$ and spiral planar [s(p)] order for $\kappa > \kappa_{\rm cl}$.

The classical spiral states themselves form two classes, one in the range $\frac{1}{6} < \kappa < \frac{1}{2}$, and the other in the range $\kappa > \frac{1}{2}$.[1–3] For the case $\frac{1}{6} < \kappa < \frac{1}{2}$ the manifold of classically degenerate spiral wave vectors comprises closed contours around the point $\mathbf{\Gamma}$. At the critical point $\kappa = \frac{1}{2}$ this closed contour described by Eq. (7) takes the form of a hexagon whose vertices are the six points $\mathbf{Q} = \mathbf{M}^{(k)}$; $k = 1, 2, \cdots, 6$, that are the centers of the six edges of the hexagonal first Brillouin zone corresponding to the honeycomb lattice. Explicitly, these are given by $(M_a, M_b) = (0, \pi)$, $(-\pi, \pi)$, $(-\pi, 0)$, $(0, -\pi)$, $(\pi, -\pi)$, and $(\pi, 0)$, for the cases $k = 1, 2, \cdots, 6$, respectively. Clearly there are only three distinct $\mathbf{M}$ vectors, which we denote as $\mathbf{M}^{*(l)}$; $l = 1, 2, 3$. They can be chosen, for example, as $(M_a^{*(l)}, M_b^{*(l)}) = (0, \pi), (\pi, 0), (\pi, \pi)$ for $l = 1, 2, 3$, respectively, which represent the midpoints of the three Brillouin zone boundaries that join at a hexagonal vertex in $\mathbf{Q}$ space.

For the case $\kappa > \frac{1}{2}$, the classically degenerate spiral wave vectors now comprise closed contours given by Eq. (7), around the six points $\mathbf{Q} = \mathbf{K}^{(k)}$; $k = 1, 2, \cdots, 6$, that are the vertices of the hexagonal first Brillouin zone. These are given explicitly by $(K_a, K_b) = (\frac{4\pi}{3}, -\frac{2\pi}{3})$, $(\frac{2\pi}{3}, \frac{2\pi}{3})$, $(-\frac{2\pi}{3}, \frac{4\pi}{3})$, $(-\frac{4\pi}{3}, \frac{2\pi}{3})$, $(-\frac{2\pi}{3}, -\frac{2\pi}{3})$, and $(\frac{2\pi}{3}, -\frac{4\pi}{3})$, respectively. When $\kappa \to \infty$, these closed contours collapse to the six points $\mathbf{Q} = \mathbf{K}^{(k)}$, which are just the wave vectors corresponding to the classical 120° ordering state on the triangular lattice, just as expected in this limit where the two sublattices of the honeycomb lattice become totally decoupled. Clearly there are only two distinct $\mathbf{K}$ vectors, which we denote as $\mathbf{K}^{*(n)}$; $n = 1, 2$. They can be chosen as $(K_a^{*(n)}, K_b^{*(n)}) = (-\frac{2\pi}{3}, -\frac{2\pi}{3})$, $(\frac{2\pi}{3}, \frac{2\pi}{3})$ for $n = 1, 2$, respectively. If we define lattice vectors $\mathbf{d}_1 = -\frac{1}{\sqrt{3}}\hat{y}$, $\mathbf{d}_2 = \frac{1}{2}\hat{x} + \frac{1}{2\sqrt{3}}\hat{y}$, and $\mathbf{d}_3 = -\frac{1}{2}\hat{x} + \frac{1}{2\sqrt{3}}\hat{y}$ to be the vectors joining a B site on the $\mathcal{B}$ sublattice to its three NN A sites on the $\mathcal{A}$ sublattice, then the six corners of the first Brillouin zone at $\mathbf{Q} = \mathbf{K}^{(i)}$ all have the property that $(\mathbf{K}^{(i)} \cdot \mathbf{d}_1, \mathbf{K}^{(i)} \cdot \mathbf{d}_2, \mathbf{K}^{(i)} \cdot \mathbf{d}_3)$ is a permutation of $(0, \frac{2\pi}{3}, \frac{4\pi}{3})$. The unit vectors joining the six NN pairs of the same sublattice (i.e., the NNN pairs on the honeycomb lattice) are $\pm\hat{b}_l$; $l = 1, 2, 3$, where $\hat{b}_1 \equiv \mathbf{d}_2 - \mathbf{d}_3 = \hat{a}$, $\hat{b}_2 \equiv \mathbf{d}_3 - \mathbf{d}_1 = \hat{b}$, and $\hat{b}_3 \equiv \mathbf{d}_1 - \mathbf{d}_2 = -\hat{a} - \hat{b}$. The two distinct $\mathbf{K}^{*(n)}$ vectors then have the property that $\mathbf{K}^{*(n)} \cdot \hat{b}_l = (-1)^n \frac{2\pi}{3}$ for $l = 1, 2, 3$.

As we mentioned in Sec. I, it has been shown[3] that in the region $\kappa > \frac{1}{6}$ $O(1/s)$ quantum corrections lift the huge classical GS degeneracy to favor specific wave vectors, i.e., to select specific points from the respective closed contours. For the case $\frac{1}{6} < \kappa < \frac{1}{2}$ the wave vectors so selected[3] are those points on the corresponding closed contours around $\mathbf{\Gamma}$ that are intersected by the six vectors $\mathbf{Q} = \mathbf{M}^{(k)}$. For the limiting case $\kappa = \frac{1}{2}$ these are just the wave vectors $\mathbf{Q} = \mathbf{M}^{(k)}$; $k = 1, 2, \cdots, 6$ themselves. The three distinct such states, denoted as $\mathbf{M}^{*(k)}$, $k = 1, 2, 3$ above are precisely the three distinct collinear Néel-II planar [N-II(p)] states, one of which, namely that with $\mathbf{Q} = \mathbf{M}^{*(1)}$, is illustrated in Fig. 1(d). They are all characterized by having ferromagnetic NN bonds in one of the three lattice directions while those in the remaining two directions are antiferromagnetic. Finally, for the case $\kappa > \frac{1}{2}$, the wave vectors selected by $O(1/s)$ quantum corrections[3] lie at the intersections of the corresponding closed contours around the corner points $\mathbf{K}^{(k)}$ of the first Brillouin zone with the edges of the zone. As κ increases from the value $\frac{1}{2}$ the selected wave vectors thus move along the edges of the border zone, starting at the center points $\mathbf{M}^{(k)}$ and moving monotonically towards the vertices $\mathbf{K}^{(k)}$ as $\kappa \to \infty$.

Our aim now is to study the XY model of Eq. (2) on the honeycomb lattice for the case $s = \frac{1}{2}$. We found previously[14,15] that for the corresponding Heisenberg model of Eq. (1) quantum fluctuations are strong enough in the spin-$\frac{1}{2}$ case to change the GS phase diagram very substantially from its classical counterpart discussed above. In particular, over the entire range $0 \le \kappa \le 1$, none of the spiral phases that are present classically for all values $\kappa > \frac{1}{6}$ form the stable GS phase for the spin-$\frac{1}{2}$ system. This finding is a particularly dramatic confirmation of the more general observation that quantum fluctuations tend to favor GS phases with collinear ordering over those, such as the spiral phases, with non-collinear order. Similarly, we also found for the spin-$\frac{1}{2}$ Heisenberg model that the Néel state is stabilized out to

a value $\kappa_{c_1} \approx 0.21$, substantially beyond the corresponding classical value $\kappa_{\rm cl} = \frac{1}{6}$. Furthermore, we found that the collinear Néel-II state, which exists as the stable GS phase for the classical J_1–J_2 Heisenberg model on the honeycomb lattice only at the highly degenerate point $\kappa = \frac{1}{2}$, provides the stable GS phase for the corresponding spin-$\frac{1}{2}$ model for values $\kappa > \kappa_{c_3} \approx 0.65 \pm 0.05$ within the window $0 \leq \kappa \leq 1$ that was examined. Over the entire range $\kappa > \kappa_{c_2} \approx 0.385 \pm 0.005$, we found a very close competition between the Néel-II state and the SDVBC (or lattice nematic) state. These two states are closely related, and indeed the latter is obtained from the former by replacing all of the NN ferromagnetic spin pairs by spin-zero dimers. Hence the two states break the lattice rotational symmetry in the same way. Results of our CCM analysis[15] provided good numerical evidence that the SDVBC state is favored as the GS phase in the region $\kappa_{c_2} < \kappa < \kappa_{c_3}$. Finally, in the region $\kappa_{c_1} < \kappa < \kappa_{c_2}$, our previous CCM analysis[14,15] strongly indicated that the stable GS phase is the PVBC state, which preserves the lattice rotational symmetry.

In view of the above results, obtained from analyses using the CCM, we now also apply the CCM to the corresponding spin-$\frac{1}{2}$ J_1–J_1 XY model of Eq. (2) on the honeycomb lattice. Since the two models of Eqs. (1) and (2) share exactly the same classical GS phase diagram (i.e., in the limit as $s \to \infty$) on the honeycomb lattice, it is of particular interest to enquire whether quantum fluctuations behave differently for the two models in the case $s = \frac{1}{2}$, where their effects are expected to be largest.

As a final point we recall that quantum spin-$\frac{1}{2}$ operators can be mapped exactly[42] onto hard-core (HC) boson operators by making the identifications,

$$s_k^+ \to b_k^\dagger \,; \quad s_k^- \to b_k \,; \quad s_k^z \to n_k - \frac{1}{2} \,, \tag{11}$$

where $s_k^\pm \equiv s_k^x \pm i s_k^y$ are the usual spin raising and lowering operators respectively, $b_k^\dagger$ and b_k are HC boson creation and annihilation operators at site k, and $n_k \equiv b_k^\dagger b_k$ is the boson number operator at site k. The imposition of the HC constraint that no more than one boson can occupy any site (viz., $n_k = 0, 1$ only) then guarantees that the bosonic Hilbert space has the same dimensionality as that of the spin-$\frac{1}{2}$ system (viz., two states per site). For the bosons we assume that operators at different sites ($k \neq l$) commute as usual,

$$[b_k^\dagger, b_l^\dagger] = [b_k, b_l] = [b_k, b_l^\dagger] = 0 \,; \quad k \neq l \,, \tag{12}$$

but to exclude multiple occupancy at any site we assume fermion-like anticommutation relations when $k = l$,

$$\{b_k, b_k\} = 0 = \{b_k^\dagger, b_k^\dagger\} \,; \quad \{b_k^\dagger, b_k\} = 1 \,. \tag{13}$$

It is easy to show from Eq. (13) that these HC bosons obey the same commutation relations with the number operator,

$$[n_k, b_k^\dagger] = b_k^\dagger \,; \quad [n_k, b_k] = -b_k \,, \tag{14}$$

as do ordinary bosons [i.e., those obeying the usual commutation relations rather than their anticommutation counterparts in Eq. (13)]. Furthermore, Eq. (13) also readily implies the commutation relation for HC bosons,

$$[b_k^\dagger, b_k] = 2n_k - 1 \,. \tag{15}$$

Thus, one observes from Eqs. (12), (14) and (15) that the mapping of Eq. (11) produces the correct SU(2) spin commutation relations,

$$[s_k^\mu, s_l^\nu] = 0 \quad \forall \, \mu, \nu \in \{+, -, z\} \,; \quad k \neq l \,, \tag{16}$$

for spins on different sites, and

$$[s_k^z, s_k^\pm] = \pm s_k^\pm \,; \quad [s_k^+, s_k^-] = 2 s_k^z \,, \tag{17}$$

for operators on the same site. The commutation relations of Eq. (17) readily yield the anticommutation relation,

$$\{s_k^+, s_k^-\} = 2s(s+1) - 2s_z^2 \,, \tag{18}$$

which, for the special case $s = \frac{1}{2}$ only, gives

$$\{s_k^+, s_k^-\} = 1 \,; \quad s = \frac{1}{2} \,. \tag{19}$$

Equation (19), together with the corresponding results $(s^+)^2 = 0 = (s^-)^2$ that hold for $s = \frac{1}{2}$, then exactly reproduce Eq. (13) under the mapping of Eq. (11).

This exact isomorphism between HC bosonic systems and quantum spin-$\frac{1}{2}$ systems on a lattice can often be used to gain additional insight into either system. The spin-$\frac{1}{2}$ J_1–J_2 XY model of Eq. (2) maps onto the particularly revealing HC boson model,

$$\mathcal{H}_{XY} = \frac{J_1}{2} \sum_{\langle i,j \rangle} (b_i^\dagger b_j + b_j^\dagger b_i) + \frac{J_2}{2} \sum_{\langle\langle i,k \rangle\rangle} (b_i^\dagger b_k + b_k^\dagger b_i) \,, \tag{20}$$

which is simply a model of frustrated hopping, involving a competition between hopping between NN and NNN pairs of sites.

In this context it is interesting to compare the above model with another archetypal model of lattice bosons, namely the Bose-Hubbard (BH) model, the Hamiltonian for which may be written in the usual form,

$$\mathcal{H}_{\rm BH} = -t_1 \sum_{\langle i,j \rangle} (b_i^\dagger b_j + b_j^\dagger b_i) + \frac{U}{2} \sum_i n_i (n_i - 1) - \mu \sum_i n_i \,, \tag{21}$$

where t_i is the NN hopping parameter, U is the on-site (Coulomb) interaction parameter (repulsive if $U > 0$), and μ is the chemical potential. In Eq. (21) the bosons obey the usual commutation rules of Eq. (12) but with those of Eq. (13) where the anticommutators are replaced by commutators. Clearly, in the HC limit $U \to \infty$, the second term in Eq. (21) forces each site to contain no more than one boson, and this term may be removed, but with the HC constraint ($n_i = 0, 1$ only) imposed

in its place. As we have seen, this constraint may be imposed by the HC boson operator relations of Eqs. (12) and (13).

We also note that the sign of the NN hopping parameter t_1 in Eq. (21) is irrelevant since the honeycomb lattice is bipartite and the operator algebra relations are invariant under the replacement $b_i \to -b_i$, as we now show explicitly. Thus, by making use of Eq. (14) and the nested commutator expansion for operator products of the form $e^{-A}Be^{A}$, it is easy to show that the unitary operator,

$$\hat{U} \equiv \exp\left(i\pi \sum_{k\in\mathcal{A}} n_k\right), \tag{22}$$

has the following mode of action on the basic HC boson operators,

$$\hat{U}^\dagger b_l \hat{U} = \epsilon_l b_l\,; \quad \hat{U}^\dagger b_l^\dagger \hat{U} = \epsilon_l b_l^\dagger\,, \tag{23}$$

where

$$\epsilon_l = \begin{cases} -1\,; & l \in \mathcal{A}\,, \\ +1\,; & l \in \mathcal{B}\,. \end{cases} \tag{24}$$

Under this unitary transformation, $\mathcal{H}_{\rm BH}$ is mapped as follows,

$$\hat{U}^\dagger \mathcal{H}_{\rm BH}(t_1, U, \mu)\hat{U} = \mathcal{H}_{\rm BH}(-t_1, U, \mu)\,. \tag{25}$$

Since $\hat{U}$ is unitary both $\mathcal{H}_{\rm BH}(t_1, U, \mu)$ and $\mathcal{H}_{\rm BH}(-t_1, U, \mu)$ have the same energy spectrum and there is a one-to-one correspondence between their eigenstates. Similarly, under $\hat{U}$, $\mathcal{H}_{XY}$ of Eq. (20) gets mapped as follows,

$$\hat{U}^\dagger \hat{\mathcal{H}}_{XY}(J_1, J_2)\hat{U} = \mathcal{H}_{XY}(-J_1, J_2)\,, \tag{26}$$

which shows that the sign of J_1 is irrelevant for this Hamiltonian.

The analog of this for the isomorphic spin-lattice model is to make a rotation of 180° about the z_s axis of the spins on one of the two sublattices, which cannot change the physics since it simply corresponds to a different choice of direction of the local axes of spin quantization. This has the effect, however, of replacing $s_i^x \to -s_i^x$, $s_i^y \to -s_i^y$ on one sublattice, which in turn shows that the replacement $J_1 \to -J_1$ does not change the physics. As indicated previously we choose $J_1 \equiv +1$ to set the energy scale (and consider the case of frustration where $J_2 > 0$).

From the mapping of Eq. (11) one sees that the role of the chemical potential μ in the BH model for lattice bosons is played by an applied magnetic field in the z_s direction ($\mu \to B_z$) for the equivalent lattice spin model. In our case, where we consider $B_z = 0$, we see that the BH Hamiltonian of Eq. (21) thus reduces in the HC limit to precisely the first term of $\mathcal{H}_{XY}$ where $t_1 \to \frac{1}{2}J_1$.

We note that $\mathcal{H}_{XY}$ of Eq. (2) commutes with the total lattice magnetization in the z_s direction, $\mathcal{M} \equiv \sum_{k=1}^{N} s_k^z$, where N is the number of lattice sites, and s_k^z now refers to a global set of spin axes rather than the local axes used later to define the order parameter M in Sec. III. For the isomorphic boson model of Eq. (20) the analogous statement is that H_{XY} commutes with the total boson number. For bipartite lattices with AFM interactions the GS phases are expected to lie in the $\mathcal{M} = 0$ sector, and the mapping of Eq. (11) thus shows that for the analogous boson lattice model we are interested in the corresponding case of half-filling, $n \equiv \langle n_k \rangle = \frac{1}{2}$.

In this context it is interesting to note that one of the characteristic features of HC bosons on a lattice with NN hopping augmented by additional off-site two-body interactions is the appearance of solid phases at half-filling ($n = \frac{1}{2}$) with either a charge-density wave (CDW) or a bond-order wave (BOW) ordering.[43–45] Whereas a CDW at half-filling is characterized by long-range order (LRO) in fluctuations in the density operator at site k,

$$\mathcal{O}_k^{\rm CDW} \equiv a\epsilon_k\left(b_k^\dagger b_k - \frac{1}{2}\right), \tag{27}$$

where ϵ_k takes opposite value on the two sublattices (viz., $\epsilon_k \equiv -1$ if $k \in \mathcal{A}$ and $\epsilon_k \equiv +1$ if $k \in \mathcal{B}$), a BOW is characterized by LRO in fluctuations in the hopping (or kinetic energy) operator at site k,

$$\mathcal{O}_k^{\rm BOW} = (1 + a\epsilon_k)\sum_{k'}(b_k^\dagger b_{k'} + b_{k'}^\dagger b_k)\,, \tag{28}$$

where the sum over k' runs over the NN sites to k. Both the CDW and BOW states thus break lattice translational symmetry. In addition the CDW state breaks particle-hole symmetry, whereas the BOW state breaks inversion symmetry.

A typical NN two-body interaction term, $V\sum_{\langle i,j\rangle} n_i n_j$ in the bosonic system, maps into a corresponding term $V\sum_{\langle i,j\rangle} s_i^z s_j^z$ in the isomorphic spin-lattice problem, and thus replaces the NN isotropic XY interaction in the first term of H_{XY} of Eq. (2) by an effective XXZ interaction. By contrast, in the present paper the NN XY interaction is frustrated by a NNN interaction of the same form. Thus, in the bosonic language, the frustration is caused not by off-site two-body interactions but by the introduction of NNN hopping between sites of the same sublattice competing with NN hopping between sites of different sublattices. It is then interesting to speculate whether such solid phases as those with CDW ordering might also occur in this case.

Clearly a CDW phase in the boson lattice system corresponds to a Néel z-aligned phase of the sort illustrated in Fig. 1(c), due to the exact mapping of Eq. (11). Interestingly, this is precisely the GS stable phase identified for the spin-$\frac{1}{2}$ J_1–J_2 XY model on the honeycomb lattice in the recent paper[39] discussed in Sec. I. For this reason we specifically include it as a candidate model state in our CCM study of this model, as discussed in Sec. III.

Finally, we note that the Hamiltonian of Eq. (20) on the honeycomb lattice is very similar to one discussed by Haldane[46] for noninteracting electrons on a honeycomb lattice in which the electronic spin degrees of freedom are suppressed, but where both NN and NNN hopping terms

are included. The NN hopping parameter t_1 is considered real, as is the case here, but the NNN hopping parameter t_2 becomes complex, $t_2 \to |t_2|e^{i\phi}$ in one direction (and hence $t_2 \to |t_2|e^{-i\phi}$ in the other). Haldane shows that such a phase factor ϕ can be induced for t_2, leaving t_1 real, by the imposition of a suitable magnetic field in the z direction perpendicular to the 2D honeycomb plane. He then shows that when $\phi \neq 0, \pi$ the model realizes a topological insulator phase (viz., an integer quantum Hall state) in its $T = 0$ GS phase diagram, apart from the Mott insulator phase that holds for $\phi = 0, \pi$. Clearly, the Haldane model[46] is simply related to our $\mathcal{H}_{XY}$ model if the spinless fermions are replaced by HC bosons and $\phi \to \pi$. This provides yet another justification for expecting that the $T = 0$ GS phase diagram of $\mathcal{H}_{XY}$ on the honeycomb lattice might hold surprises in store.

In Sec. III we now describe the CCM technique employed here, together with the choice of model states suggested by our discussion of the model above.

III. THE COUPLED CLUSTER METHOD

The CCM has been very successfully employed for a wide variety of quantum many-body systems (see, e.g., Refs. 47–51), where it typically yields results of accuracy better than or comparable to those of alternative techniques. In recent years it has been widely applied, for example, to investigate the GS phase structure of many spin-lattice models, especially 2D ones, of interest in quantum magnetism (see, e.g., Refs. 7, 12–15, 18–38, 51, and 52, and references cited therein). The general consensus is that it now provides one of the most accurate methods available to study such models. In particular, the CCM offers a systematic technique for the investigation of various possible GS phases, including an accurate determination of the associated QCPs that demarcate their regions of stability. Very importantly, since it is formulated with well-defined hierarchies of approximations, which we describe below, it is capable of systematic improvement in accuracy, albeit at an increasing computational cost.

The CCM, as we explain below, offers a size-extensive method in which we work from the outset in the thermodynamic (i.e., infinite-lattice) limit ($N \to \infty$). Hence, no finite-size scaling is ever required. However, what it does require is for us to select a suitable, normalized model (or reference) state $|\Phi\rangle$, with respect to which the quantum correlations in the exact GS phase under study may then be explicitly included, in principle exactly, via a correlation operator, S, chosen as described below (and see e.g., Refs. 19, 49–51, and references cited therein). In the present study we use, separately, each of the N(p), N(z), and N-II(p) states shown in Figs. 1(b)-(d), respectively, as our choices for CCM model states. Each of these states is characterized as being an independent-spin product state, in which the choice of state for the spin on every site is formally independent of the choice for that of all others.

In order to make the subsequent computational implementation of the technique as universal (i.e., as independent of the choice of model state) as possible, so that every lattice site can then be treated on an equal basis, we then choose local coordinate frames in spin space for each model state we employ. The choice is made so that on each lattice site in each model state the spin aligns along, say, the negative z_s axis (henceforth called the downward) direction in its own spin-coordinate frame. Such canonical passive rotations leave the SU(2) commutation relations unchanged, and hence have no physical consequences.

We denote the exact, fully correlated, GS ket- and bra-state wave functions of the phase of the system under study as $|\Psi\rangle$ and $\langle\tilde{\Psi}|$, respectively. They satisfy the respective GS Schrödinger equations,

$$H|\Psi\rangle = E|\Psi\rangle\,; \quad \langle\tilde{\Psi}|H = E\langle\tilde{\Psi}|\,, \tag{29}$$

and their normalizations are chosen so that $\langle\tilde{\Psi}|\Psi\rangle = \langle\Phi|\Psi\rangle = \langle\Phi|\Phi\rangle = 1$. The CCM then employs the distinctive exponential parametrizations of the exact ket and bra states with respect to the corresponding chosen model state, as

$$|\Psi\rangle = e^S|\Phi\rangle\,; \qquad \langle\tilde{\Psi}| = \langle\Phi|\tilde{S}e^{-S}\,, \tag{30}$$

which are one of the hallmarks of the method. The two correlation operators, S and $\tilde{S}$ are now decomposed formally as

$$S = \sum_{I\neq 0} \mathcal{S}_I C_I^+\,; \qquad \tilde{S} = 1 + \sum_{I\neq 0} \tilde{\mathcal{S}}_I C_I^-\,, \tag{31}$$

where we define $C_0^+ \equiv 1$ to be the identity operator, and where the set-index I represents a particular set of lattice sites. It is used, as we discuss below, to denote a multispin-flip configuration with respect to the model state $|\Phi\rangle$, such that $C_I^+|\Phi\rangle$ represents the corresponding wave function for this configuration of spins. The operators C_I^+ and $C_I^- \equiv (C_I^+)^\dagger$ are thus creation and destruction operators, respectively, with respect to the model state $|\Phi\rangle$ considered as a generalized vacuum state. They are chosen so as to obey the corresponding relations,

$$\langle\Phi|C_I^+ = 0 = C_I^-|\Phi\rangle\,; \quad \forall I \neq 0\,. \tag{32}$$

The set $\{C_I^+\}$ thus forms a mutually commuting, complete set of multispin creation operators with respect to the model state $|\Phi\rangle$ as the corresponding cyclic vector.

We now discuss the choice of set-indices $\{I\}$ and creation operators $\{C_I^+\}$ in more detail for the specific case of spin-lattice models considered here. With our choice of local spin-coordinate frames as descried above, in which any independent-spin product model state has the universal form $|\Phi\rangle = |\downarrow\downarrow\downarrow\cdots\downarrow\rangle$ with all spins pointing down, the operators C_I^+ also take a universal form. Thus, $C_I^+ \to s_{l_1}^+ s_{l_2}^+ \cdots s_{l_n}^+$, a product of single-spin

raising operators, $s_l^+ \equiv s_l^x + is_l^y$, where the set-index $I \to \{l_1, l_2, \cdots, l_n;\ n = 1, 2, \cdots, 2sN\}$, a set of (possibly repeated) lattice site indices, where $N(\to \infty)$ is the total number of sites. Clearly, in the general case, for arbitrary spin quantum number s, a spin raising operator s_l^+ can be applied no more than $2s$ times on a given site l. Therefore, a given site-index l may appear no more than $2s$ times in any set-index I included in the sums in Eq. (31). Thus, for our present study, where $s = \frac{1}{2}$, each site-index l_k included in any set-index I may appear no more than once.

The CCM correlation coefficients, $\{\mathcal{S}_I, \tilde{\mathcal{S}}_I\}$, in terms of which an arbitrary GS property may formally be expressed, are themselves now calculated by minimizing the GS energy expectation functional,

$$\bar{H} = \bar{H}\{\mathcal{S}_I, \tilde{\mathcal{S}}_I\} \equiv \langle \Phi | \tilde{S} e^{-S} H e^{S} | \Phi \rangle \,, \tag{33}$$

with respect to each of the coefficients $\{\tilde{\mathcal{S}}_I, \mathcal{S}_I;\ \forall I \neq 0\}$. Equations (31) and (33) thus yields the coupled sets of equations,

$$\langle \Phi | C_I^- e^{-S} H e^{S} | \Phi \rangle = 0 \,; \quad \forall I \neq 0 \,, \tag{34}$$

by minimization with respect to $\tilde{\mathcal{S}}_I$, and

$$\langle \Phi | \tilde{S} e^{-S} [H, C_I^+] e^{S} | \Phi \rangle = 0 \,; \quad \forall I \neq 0 \,, \tag{35}$$

by minimization with respect to $\mathcal{S}_I$. Once Eq. (34) is satisfied, the GS energy, which is the value of $\bar{H}$ at the minimum, may be simply expressed as

$$E = \langle \Phi | e^{-S} H e^{S} | \Phi \rangle \,, \tag{36}$$

and Eq. (35) may be written equivalently as

$$\langle \Phi | \tilde{S} (e^{-S} H e^{S} - E) C_I^+ | \Phi \rangle = 0 \,; \quad \forall I \neq 0 \,. \tag{37}$$

The CCM equations (34) for the ket-state correlation coefficients $\{\mathcal{S}_I\}$ comprise coupled sets of nonlinear equations, due to the presence of the operator S in the exponentials. However, a key feature of the CCM is that in the equations we utilize for solution, S only appears in the combination $e^{-S} H e^{S}$, a similarity transform of the Hamiltonian. In turn, this form may be expanded in terms of the well-known nested commutator sum. Another key feature of the CCM is that this otherwise infinite sum actually terminates *exactly* with the double commutator term, due firstly to the fact that all of the terms in Eq. (31) comprising S mutually commute and are simple products of spin-raising operators, as described above, and secondly to the basic SU(2) commutator relations (and see, e.g., Refs. 19 and 22 for further details). Similar exact terminations occur for the GS expectation value of any physical operator, such as the magnetic order parameter, which is defined to be the average local on-site magnetization,

$$\begin{aligned} M &\equiv -\frac{1}{N} \langle \tilde{\Psi} | \sum_{k=1}^{N} s_k^z | \Psi \rangle \\ &= -\frac{1}{N} \langle \tilde{\Phi} | \tilde{S} \sum_{k=1}^{N} e^{-S} s_k^z e^{S} | \Phi \rangle \,, \end{aligned} \tag{38}$$

where s_k^z is defined with respect to the local rotated spin-coordinate frame on each lattice site k, as described above, and as opposed to the global spin-coordinate frame used to define the total lattice magnetization $\mathcal{M}$ in Sec. II.

We note too that the CCM parametrizations of Eqs. (30) and (31), which imply, for example, that every term in S commutes with all of the others, together with the nested commutator expansion for $e^{-S} H e^{S}$ in Eq. (34), suffice completely to show rather readily[50] that the CCM exactly obeys the Goldstone linked cluster theorem at *any* level of approximation involving truncations on the index-set $\{I\}$ retained in the sums in Eq. (31). Similarly, one can also show[50] that the CCM obeys the important Hellmann-Feynman theorem at all such levels of approximation.

Once an approximation has been made as to which multispin-flip configurations $\{I\}$ to retain in the expansions of Eq. (31) for the CCM correlation operators S and $\tilde{S}$, no further approximation is made. The set of nonlinear equations (34) for the coefficients $\{\mathcal{S}_I\}$ is first solved. They are then used as input to solve the linear set of equations (35) or (37) for the coefficients $\{\tilde{\mathcal{S}}_I\}$. Any GS expectation value may then be exactly computed at the same level of approximation. In this work we use the well-tested localized (lattice-animal-based subsystem) LSUBm truncation scheme,[19–38,51,52] which has been applied with considerable success to many different 2D spin-lattice models. At the mth level of approximation in the LSUBm scheme we retain all multispin-flip configurations $\{I\}$ defined over m or fewer contiguous lattice sites. The configurations of spins (or clusters) retained are defined to be contiguous when every site in the configuration is adjacent (i.e., as a NN) to at least one other site in the configuration. The interested reader is referred to the literature (see, e.g., Ref. 19) for specific examples that illustrate the LSUBm scheme in some detail.

Even after all space- and point-group symmetries of the lattice and the CCM model state used are taken fully into account, the number N_f of such distinct fundamental configurations that are retained in the LSUBm scheme grows rapidly with increasing values of the truncation index m. It thus becomes necessary to use massive parallelization together with supercomputing resources[19,53] for the higher-order approximations. In the present case we have been able to perform CCM calculations up to the LSUB10 level based on the N(z) model state, and up to the LSUB12 level based on both the N(p) and N-II(p) model states. For example, for the N-II(p) state the number of fundamental configurations at the LSUB12 level is $N_f = 818300$.

Since we work from the outset in the infinite-lattice ($N \to \infty$) limit, the only extrapolation we need finally to make is to take the $m \to \infty$ limit in the LSUBm truncation index, where our results are, in principle, *exact*, since we make no other approximations. For example, the LSUBm values for the GS energy per spin, $E(m)/N$,

always converge very rapidly, and we use the very well-tested extrapolation scheme[7,15,20–27,29,32,34,36–38]

$$E(m)/N = a_0 + a_1 m^{-2} + a_2 m^{-4} \,. \tag{39}$$

By contrast, but as expected, other GS quantities converge less rapidly than does the energy. For example, the magnetic order parameter, M, defined in the local spin coordinates by Eq. (38), typically follows a scheme with leading exponent $1/m$,

$$M(m) = b_0 + b_1 m^{-1} + b_2 m^{-2} \,, \tag{40}$$

for most systems studied to date that are either unfrustrated or contain only moderate amounts of frustration.[20–23,37,38] Conversely, when the system is close to a QCP or when the magnetic order parameter of the phase under study is either zero or close to zero, the scheme of Eq. (40) is usually found to overestimate the magnetic order present and/or to yield a somewhat too large value for the critical strength of the frustrating interaction that is driving the corresponding phase transition. In such cases a scheme with leading exponent $1/m^{1/2}$,

$$M(m) = c_0 + c_1 m^{-1/2} + c_2 m^{-3/2} \,, \tag{41}$$

has then usually been found both to fit the LSUBm results much better and to yield more accurate QCPs.[7,15,25–38]

In general, of course, one may always test for the correct leading exponent ν for the extrapolation scheme for any GS physical quantity Q,

$$Q(m) = q_0 + q_1 m^{-\nu} \,, \tag{42}$$

by fitting an LSUBm sequence of results $\{Q(m)\}$ to this form, with each of the parameters q_0, q_1, and ν treated as fitting parameters.[15,21,23,37,38] For the present model we have performed fits of the form of Eq. (42) for both the GS energy per spin, E/N, and the magnetic order parameter, M, as described in Sec. IV. For the energy we find fitted values of ν close to 2, and thereafter use Eq. (39) to do the final extrapolations. Similar fits of the form of Eq. (42) for M have been performed before using a final extrapolation scheme of either of the forms of Eqs. (40) and (41), as appropriate.

In Sec. IV we first present our CCM LSUBm results in the range $0 \leq \kappa \leq 1$ for the GS quantities E/N and M, together with their corresponding $m \to \infty$ extrapolations, based on each of the model states N(p), N(z), and N-II(p) separately. Since LSUB2 results are generally too far away from the asymptotic limit, we perform all extrapolations with $m \geq 4$. Furthermore, since the hexagon is such a basic structural element of the lattice we generally prefer to do extrapolations with values of the truncation index $m \geq 6$, whenever possible and, in particular, when not in conflict with the clear preference that any LSUBm extrapolation scheme with n fitting parameters should best be fitted with more than n corresponding LSUBm results.

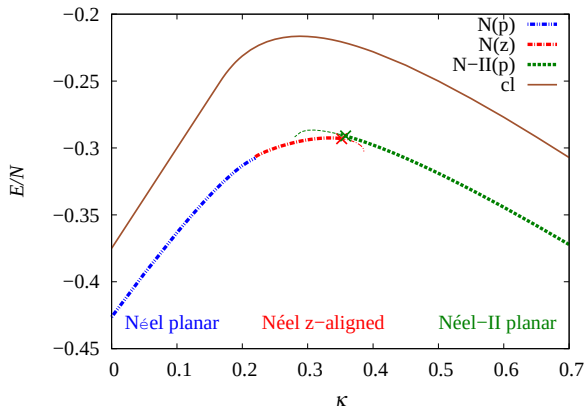

FIG. 2. (Color online) Extrapolated CCM LSUB∞ results for the GS energy per spin E/N versus the frustration parameter $\kappa \equiv J_2/J_1$, for the spin-$\frac{1}{2}$ J_1–J_2 isotropic XY model on the honeycomb lattice (with $J_1 = 1$). We show results based on the Néel planar [N(p)], the Néel z-aligned [N(z)], and the Néel-II planar [N-II(p)] states as CCM model states. The extrapolated LSUB∞ curves shown are all based on Eq. (39), using LSUBm results with $m = \{6, 8, 10, 12\}$ for the N(p) and N-II(p) states, and with $m = \{4, 6, 8, 10\}$ for the N(z) state. The times ($\times$) symbols mark the points where the respective extrapolations for the order parameter have $M \to 0$, and the unphysical portions of the solutions beyond those points (i.e., where $M < 0$) are shown by thinner lines (and see text for details). Also shown for comparison is the corresponding classical (cl) result from Eqs. (6) and (10), using the value $s = \frac{1}{2}$.

IV. RESULTS

In Fig. 2 we present our extrapolated CCM results for the GS energy per spin, E/N, of the spin-$\frac{1}{2}$ Hamiltonian $\mathcal{H}_{XY}$ on the honeycomb lattice, where we have put $J_1 \equiv +1$ and $\kappa \equiv J_2/J_1$. Results are shown for the three separate cases of the Néel planar [N(p)], Néel z-aligned [N(z)], and the Néel-II planar [N-II(p)] states shown in Figs. 1(b), (c) and (d) respectively, used as CCM model states. For comparison purposes we also show the corresponding classical result in Fig. 2, taken from Eqs. (6) and (10) with the spin quantum number set to the value $s = \frac{1}{2}$.

We do not display in Fig. 2 the data for the individual LSUBm approximations since on the scale shown the corresponding results based on the same model state lie almost on top of each other, exactly as was observed in our previous work for the comparable Heisenberg model of Eq. (1) (and see, e.g., Fig. 2 of Ref. 15). Due to this rapid convergence of the LSUBm energy curves with increasing values of the truncation index m, for CCM results based on the same model state, we show in Fig. 2 only the corresponding extrapolated LSUB∞ results based on Eq. (39), which, as is usually the case, fits the LSUBm data well for each of the three model states used.

We note that for all three model states results are shown in Fig. 2 only over certain well-defined specific

ranges of the frustration parameter, κ. All three curves display termination points, namely an upper one for the N(p) curve, both an upper and a lower one for the N(z) curve, and a lower one for the N-II(p) curve. In turn these termination points are manifestations of the corresponding termination points in the LSUBm results, which themselves depend on the truncation index m. As is generally the case we find here that as the index m is increased the range of values of κ for which the respective LSUBm equations (based on a specific model state) for the CCM correlations coefficients $\{\mathcal{S}_I, \tilde{\mathcal{S}}_I\}$ have real solutions, becomes narrower. The termination points shown on the LSUB∞ curves for E/N in Fig. 2 are precisely those of the LSUBm solution with the highest value of the truncation index m used in the corresponding extrapolation.

Such termination points of LSUBm CCM solutions are very common in many other applications of the technique. They have been studied in detail and are, by now, well understood (see, e.g., Refs. 28, 29, and 51). They are always direct manifestations of the corresponding QCP in the physical system being studied, at which the order associated with the corresponding model state melts. Hence the values $\kappa_t(m)$ of the termination points for a particular end of a specific branch of CCM LSUBm solutions may, in principle, be used to estimate the corresponding QCP for that GS phase under study, as $\kappa_c = \lim_{m\to\infty} \to \kappa_t(m)$. On the other hand it is the case that the number of iterations required to solve the CCM LSUBm equations to a given accuracy increases significantly as $\kappa \to \kappa_t(m)$. Since it is correspondingly costly, in terms of computational resources, to obtain the values $\kappa_t(m)$ with the high precision necessary for accurate extrapolations, we do not employ this method for determining the QCPs in the present model, since we have other more accurate criteria available to us here, as we describe below.

As is generally the case we find here too for the present XY model that the CCM LSUBm results for finite values of m based on the same specified model state for each of the three states, employed here, extend beyond the corresponding LSUB∞ termination points (which are thus the respective QCPs). The actual LSUBm termination points for larger values of m can sometimes lie very close to the corresponding QCP at which the phase under study melts. This is particularly striking for the present XY model for the corresponding upper termination point for the N(p) LSUBm results and the lower termination point for the N(z) LSUBm results, both of which converge very rapidly as m is increased to what appears to be the *same* value of $\kappa_{c_1} \approx 0.22$, as can clearly be seen from Fig. 2. It is also particularly noteworthy from Fig. 2 that both corresponding LSUB∞ curves based on the N(p) and N(z) states as model states apparently meet both continuously and smoothly at this value $\kappa = \kappa_{c_1}$. Thus, based on our GS energy results alone we have preliminary, but rather strong, evidence that the model has a first QCP at $\kappa_{c_1} \approx 0.22$ from N(p) to N(z) order. The evidence from Fig. 2 points strongly towards a direct $T = 0$ second-order (continuous) quantum phase transition at κ_{c_1}, at which both the energy and its first derivative with respect to κ appear to be continuous within very small error bars.

In order to analyze the other termination points displayed in Fig. 2 (viz., the upper termination point of the N(z) branch and the lower termination point of the N-II(p) branch) we first make some additional general remarks about the behavior of the real CCM solution branches near termination points $\kappa_t(m)$. As has been observed many times previously (and see, e.g., Ref. 38), we also find for the present XY model that for a region near $\kappa_t(m)$ the respective real CCM LSUBm solution can itself become unphysical in the sense that the corresponding order parameter (viz., the local average on-site magnetization, M, here) now takes negative values. The points on the energy curves in Fig. 2 where $M \to 0$, (which we determine as discussed below) are shown as times ($\times$) symbols, and the corresponding (unphysical) regions beyond those points, where $M < 0$, are shown by thinner portions of the curves than the respective (physical) regions where $M > 0$, which are denoted by the thicker portions.

We note from Fig. 2 that the upper critical point for the N(z) phase beyond which its order parameter M becomes negative is at $\kappa \approx 0.352$, while the corresponding lower critical point for the N-II(p) phase below which its order parameter becomes negative is at $\kappa \approx 0.358$. However, as we discuss in more detail below, there is more uncertainty associated with the latter value. While the two energy curves for the N(z) and N-II(p) phases do not meet quite as precisely as do those for the N(p) and N(z) phases, there is clear evidence from the energy results alone of a second QCP at $\kappa_{c_2} \approx 0.36$. Nevertheless, the energy per spin in the N-II(p) phase is still slightly *above* that of the N(z) phase at this point, and we consider this difference to be outside the errors in our results. The simplest explanation for these results is that an intermediate phase exists as the stable GS phase for the system in the range $\kappa_{c_2} < \kappa < \kappa_{c_3}$, where κ_{c_3} is as yet undetermined, and where the N-II(p) phase only becomes the lowest-energy stable GS phase (at $T = 0$) for $\kappa > \kappa_{c_3}$. We return to this point after discussing our corresponding CCM results for the order parameter, M, for the same three phases as shown in Fig. 2 for the energy.

Before doing so, however, we comment briefly on the accuracy of our CCM results. For example, for the case of zero frustration ($\kappa = 0$) with NN isotropic XY interactions only, our extrapolated CCM value for the GS energy per spin is $E(\kappa = 0)/N \approx -0.4263$ based on LSUBm results with $m = \{6, 8, 10, 12\}$ and the standard extrapolation scheme of Eq. (39). This may be compared with value $E(\kappa = 0)/N = -0.4261(1)$ from a high-order linked-cluster series expansion (SE) analysis of the model around the Ising limit.[54] Similarly, at the value $\kappa = 0.3$, which is around the center of the range where the N(z) phase appears to be the stable GS phase,

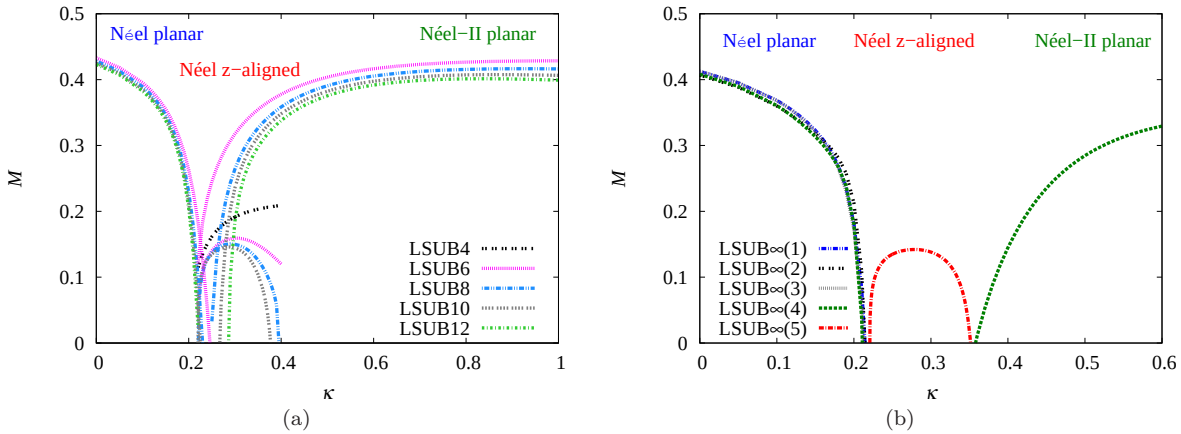

FIG. 3. (Color online) CCM results for the GS magnetic order M versus the frustration parameter $\kappa \equiv J_2/J_1$ for the spin-$\frac{1}{2}$ J_1–J_2 isotropic XY model on the honeycomb lattice (with $J_1 > 0$). We show results based on the Néel planar [N(p)], the Néel z-aligned [N(z)], and the Néel-II planar [N-II(p)] states as CCM model states. (a) LSUBm results are shown with $m = \{6, 8, 10, 12\}$ for the N(p) and N-II(p) states, and with $m = \{4, 6, 8, 10\}$ for the N(z) state. (b) Extrapolated LSUB$\infty(k)$ results are shown for the N(p) state using both the schemes of Eq. (40) with $k = 1, 3$ and Eq. (41) with $k = 2, 4$, where the LSUB$\infty(k)$ curves with $k = 1, 2$ are based on LSUBm results with $m = \{6, 8, 10, 12\}$ and those with $k = 3, 4$ are based on those with $m = \{8, 10, 12\}$. For the N(z) state the LSUB$\infty(5)$ curve is based on Eq. (42), using the LSUBm data set, $m = \{4, 6, 8, 10\}$. For the N-II(p) state we show only the LSUB$\infty(4)$ curve, defined as above.

and which is also close to the point $\kappa = 1/\sqrt{12} \approx 0.2887$ where the classical energy is maximal, our corresponding extrapolated CCM result is $E(\kappa = 0.3)/N \approx -0.2947$. This may be compared with the recent estimated value $E(\kappa = 0.3)/N = -0.2945(1)$ for the infinite 2D limiting case, based on large-scale density-matrix renormalization group (DMRG) calculations on wide cylinders.[39] Both of our values are in excellent agreement at these two points with the best results available by other techniques. Exact diagonalization (ED) results on 24-site clusters (comprising a $4 \times 2 \times 2$ torus) are also available,[55] yielding values $E(\kappa = 0)/N = -0.42941$ and $E(\kappa = 0.3)/N = -0.29528$, for example, which are also close to our values but which lie lower in energy than ours by about 0.7% and 0.2% respectively, presumably due to finite-size effects.

We now turn to our corresponding CCM results for the order parameter M, and we show in Fig. 3 the values obtained using the same three model states as shown in Fig. 2 for the energy. From Fig. 3(a) we observe that the LSUBm results converge extremely rapidly with increasing order m of approximation for the N(p) phase, and each of the curves tends to zero around the same value of κ (near κ_{c_1}) with almost vertical slope. The same is also true for the LSUBm results near κ_{c_1} for the N(z) phase. It is precisely for this reason that the corresponding LSUBm branches of solutions based on both the N(p) and N(z) model states terminate at values very close to the points at which the solutions become unphysical in the sense of yielding negative values for the order parameter, and hence why in Fig. 2 the corresponding energy curves near κ_{c_1} display no perceptible "unphysical" regions shown as thinner portions of the curves. By contrast, the LSUBm results for the N(z) phase near the upper critical point converge more slowly than near the lower critical point, as do the overall results for the N-II(p) phase, especially near the (lower) critical point at which the N-II(p) order melts. These latter observations thus provide the reason for why the N(z) and N-II(p) curves shown in Fig. 2 illustrate the "unphysical" regions (shown as thinner portions of the corresponding curves) extending beyond the points where the respective extrapolated values of the order parameter M have vanished.

In Fig. 3(b) we show extrapolated results for the order parameter of the three states used as CCM model states, based on the raw LSUBm results shown in Fig. 3(a). We note firstly that for the N(p) phase the extrapolated results are extremely insensitive both to the choice of extrapolation scheme from either Eq. (40) or Eq. (41), and to the LSUBm data set used. For example, for the unfrustrated limiting case, $\kappa = 0$, when Eq. (40) is the appropriate extrapolation scheme, we obtain extrapolated LSUB∞ values $M(\kappa = 0) \approx 0.4125$ when the LSUBm data set $m = \{6, 8, 10, 12\}$ is used, and $M(\kappa = 0) \approx 0.4127$ with the corresponding set $m = \{8, 10, 12\}$. These values may again be compared with, and seen to be in excellent agreement with, the result $M(\kappa = 0) = 0.4133(3)$ from a high-order SE analysis of the model.[54] We have no reason to believe that our results will be any less accurate at other values of κ.

We observe from Fig. 3(b) again the extreme insensitivity of the N(p) results to the choice of extrapolation scheme, even for the corresponding estimates for the QCP κ_{c_1} at which the respective values for M vanishes in this phase. For example, using Eq. (41), which is the appropriate choice in this regime of maximal frustration for the N(p) phase we obtain values $\kappa_{c_1} \approx 0.214$ using

the LSUBm data set $m = \{6, 8, 10, 12\}$, and $\kappa_{c_1} \approx 0.211$ with the corresponding set $m = \{8, 10, 12\}$.

By contrast with the results for the N(p) phase where we have LSUBm results with $m = \{6, 8, 10, 12\}$, for the N(z) phase we have LSUBm results only for values $m \leq 10$. In this case it seems clearly preferable to use the totally unbiased extrapolation scheme of Eq. (42) for the order parameter M, where the exponent ν is itself a fitting parameter. The corresponding LSUB∞ extrapolated result is shown in Fig. 3(b) for the N(z) phase, based on our LSUBm results with $m = \{4, 6, 8, 10\}$. The respective value for the lower QCP at which N(z) order melts is thereby obtained as $\kappa \approx 0.221$. The same value is obtained using the set $m = \{6, 8, 10\}$. Thus, the values of the respective critical points at which both N(p) and N(z) forms of order melt are essentially identical, and from the shape of the curves and, indeed, from all of our results so far, there is very strong evidence for a lower QCP at $\kappa_{c_1} = 0.216(5)$ at which a second-order (continuous) phase transition occurs between a state with N(p) order (for $0 \leq \kappa < \kappa_{c_1}$) and one with N($z$) order immediately above κ_{c_1}.

The GS phase with N(z) order is then seen from Fig. 3(b) to obtain a maximal value of its order parameter, $M \approx 0.142$, at $\kappa \approx 0.279$, which is very close to the point $\kappa = 1/\sqrt{12} \approx 0.289$ where the classical version of the model has the energy taking its maximal value. We may also compare our own result in this phase at the point $\kappa = 0.3$, viz., $M(\kappa = 0.3) \approx 0.138$, with the recent estimate[39] $M(\kappa = 0.3) \sim 0.14$ for the extrapolated 2D infinite-lattice limit, based on large-scale DMRG calculations on wide cylinders. Finally, for this stable N(z) phase, as κ is increased further, our extrapolated LSUB∞ result shown in Fig. 3(b) provides a value $\kappa \approx 0.352$ for the upper QCP at which the N(z) order melts.

Figure 3 also presents CCM results for M based on the model state with N-II(p) ordering. Even a simple inspection by eye of the individual LSUBm results for this case, shown in Fig. 3(a), shows that the LSUB6 results appear anomalous, in the sense that they do not fit with a leading-order extrapolation scheme of the form of Eq. (42) with *any* value for the exponent ν. By contrast, those LSUBm results with $m > 6$ are accurately fitted by such a scheme with a fitted value of ν close to 0.5, as expected in this highly frustrated regime, over the whole range of values for κ shown. Quite why the LSUBm result with $m = 6$ should be anomalous for this phase is not obvious. Very interestingly, however, exactly the same behavior occurred for the LSUB6 results in our prior study[15] of the Néel-II phase of the corresponding spin-$\frac{1}{2}$ J_1–J_2 Heisenberg model of Eq. (1) on the honeycomb lattice. It is for these reasons that in Fig. 3(b) we show for the N-II(p) phase the extrapolated LSUB∞ result for M based on Eq. (41) and on the LSUBm data set $m = \{8, 10, 12\}$ alone. The corresponding estimate for the point below which N-II(p) order vanishes is $\kappa \approx 0.358$, which is in very close agreement with our estimate $\kappa \approx 0.352$ for the point above which N(z) order vanishes. Again, all of our results for M to date indicate the presence in this model of a second QCP at $\kappa_{c_2} \approx 0.355(5)$ between a N(z)-ordered phase for $\kappa_{c_1} \leq \kappa < \kappa_{c_2}$ and a N-II(p)-ordered phase for $\kappa > \kappa_{c_2}$.

It is interesting to note that although the LSUB∞ curve for M for the N(z) phase approaches zero at κ_{c_2} with a very steep slope, indicative of a second-order transition, the corresponding curve for the N-II(p) phase approaches zero at κ_{c_2} with a shallower slope. On the other hand, the individual LSUBm curves for the N-II(p) phase do approach zero somewhat more steeply. These observations indicate that the extrapolation of the N-II(p) results is likely to be rather sensitive in the region around the corresponding QCP. Since the individual LSUBm curves approach zero with increasingly steep gradients as m increases, as seen from Fig. 3(a), it seems entirely likely that the LSUB∞ curve should perhaps approach zero with infinite (or very large) slope. In this case the actual extrapolated value, κ_{c_3}, of the QCP below which N-II(p) order melts would likely be greater than the value κ_{c_2} above which N(z) order melts. In this case there would be an additional intermediate phase in the regime $\kappa_{c_2} < \kappa < \kappa_{c_3}$. Such a scenario is entirely consistent with our previous energy results in Fig. 2 which seem to show that at κ_{c_2} the N-II(p) state still has a slightly higher energy than the N(z) state.

The question thus arises as to what might be the nature of such an intermediate state. Since real CCM LSUBm solutions with finite values of m based on the N-II(p) model state clearly persist well into any such intermediate region, one might therefore expect that the actual GS phase in this region shares some distinct similarities with the N-II(p) state. One such obvious state is the so-called staggered dimer valence-bond crystalline (SDVBC) state, also known as a lattice nematic state, which has also been observed as a stable $T = 0$ GS phase of the analogous spin-$\frac{1}{2}$ J_1–J_2 Heisenberg model of Eq. (1) on the honeycomb lattice.[15] Both the N-II(p) and the SDVBC states break the lattice rotational symmetry in exactly the same way, since the SDVBC state is basically obtained from the N-II(p) state by replacing all of the NN parallel pairs of spins by spin-singlet dimers, as illustrated in Fig. 4(a)

A convenient way to test for the susceptibility of a candidate GS phase built on a particular CCM model state is to consider its response to the imposition of a field operator F (see Ref. 27) exactly as we did previously[15] for the corresponding case of the spin-$\frac{1}{2}$ J_1–J_2 Heisenberg model of Eq. (1) on the honeycomb lattice. We thus add an extra field term $F = \delta\, \hat{O}_d$ to the Hamiltonian of Eq. (2), where the operator $\hat{O}_d$ now corresponds to the promotion of SDVBC order, as illustrated schematically in Fig. 4(a) and as defined specifically in the figure caption, and where δ is ultimately taken as an infinitesimal parameter.

The perturbed energy per site, $e(\delta) \equiv E(\delta)/N$, is then calculated at various LSUBm levels of approximation,

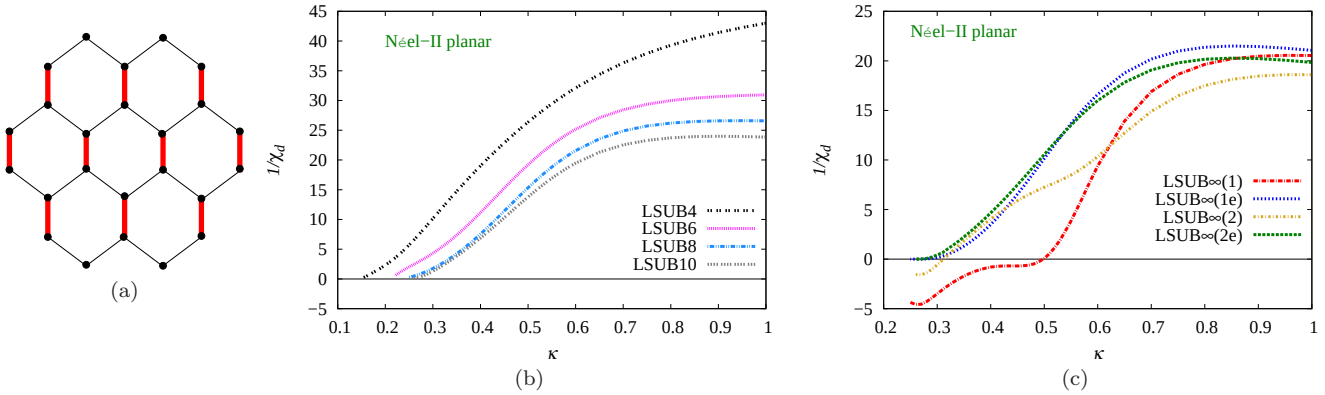

FIG. 4. (Color online) (a) The perturbing field $F \to \delta \hat{O}_d\,, \delta > 0$, for the staggered dimer susceptibility, χ_d. Thick (red) and thin (black) lines correspond respectively to strengthened and unaltered NN exchange couplings, where $\hat{O}_d = \sum_{\langle i,j \rangle} a_{ij} \mathbf{s}_i \cdot \mathbf{s}_j$, and the sum on $\langle i,j \rangle$ runs over all NN bonds, with $a_{ij} = +1$ for thick (red) lines and $a_{ij} = 0$ for thin (black) lines. (b) CCM LSUBm results with $m = \{4, 6, 8, 10\}$ for $1/\chi_d$ versus the frustration parameter $\kappa \equiv J_2/J_1$ for the spin-$\frac{1}{2}$ J_1–J_2 isotropic XY model on the honeycomb lattice (with $J_1 > 0$), using the Néel-II planar state as model state. (c) The corresponding extrapolated LSUB∞(ke) and LSUB∞(k) results, based on Eqs. (44) and (45) respectively, are shown, in each case using both the LSUBm data sets: $k = 1$, $m = \{4, 6, 8\}$ and $k = 2$, $m = \{4, 6, 8, 10\}$.

using the N-II(p) state as model state, for the infinitesimally shifted Hamiltonian $H + F$. The corresponding susceptibility of the system to this perturbation is then defined, as usual, as

$$\chi_d \equiv - \left. \frac{\partial^2 e(\delta)}{\partial \delta^2} \right|_{\delta=0} . \tag{43}$$

The GS phase will thus become unstable against the formation of SDVBC order when $\chi_d \to \infty$ or, equivalently, when $\chi_d^{-1} \to 0$. Our LSUBm results for χ_d^{-1} are plotted in Fig. 4(b) for $m = \{4, 6, 8, 10\}$, using the N-II(p) state of Fig. 1(d) as the CCM model state. We see clearly by a comparison of Figs. 3(a) and 4(b) that in each case χ_d^{-1} approaches zero at a value of κ that corresponds closely to the corresponding point at which $M \to 0$ at the same LSUBm level. It is also noteworthy that at each LSUBm level, the curve for χ_d^{-1} tends to zero at a rather shallow angle, and that the intercept slope at this point decreases as the truncation parameter m increases.

Nevertheless, our LSUBm results for χ_d (or χ_d^{-1}) still need to be extrapolated to the physical (LSUB∞) limit. The simplest and most direct way to do so[37,38] is to extrapolate first the LSUBm results for the perturbed energy per spin, $e(\delta)$, using an unbiased scheme of the form of Eq. (42), namely

$$e^{(m)}(\delta) = e_0(\delta) + e_1(\delta) m^{-\nu} , \tag{44}$$

where each of $e_0(\delta)$ and $e_1(\delta)$, and ν are treated as fitting parameters. Since our standard LSUBm extrapolation scheme for the GS energy is as given in Eq. (39), as discussed in Sec. III, our expectation is that the fitted value of ν in Eq. (44) should be close to the value 2. This has usually been observed to be the case in previous applications, except possibly near or inside any critical regime for the phase under consideration, where it can deviate significantly from this value (and see, e.g., Ref. 38 for a discussion of a specific example of such behavior). An alternative extrapolation scheme[7,37,38] is to use the LSUBm results for the quantity χ_d^{-1} itself, again with an unbiased scheme of the form of Eq. (42), namely

$$\chi_d^{-1}(m) = y_0 + y_1 m^{-\nu} , \tag{45}$$

with y_0, y_1, and ν treated as fitting parameters. Corresponding extrapolations using some or all of the LSUBm results shown in Fig. 4(b) are displayed in Fig. 4(c), using each of Eqs. (44) and (45), where they are labelled as LSUB∞(ke) and LSUB∞(k), respectively, and where the index k denotes the LSUBm data set used in the corresponding extrapolation.

We note from Fig. 4(b) that the LSUB10 results for χ_d^{-1} appears somewhat anomalous in the region $\kappa \lesssim 0.5$ in the sense that they lie closer than expected to the LSUB8 results by contrast with the spacings of the LSUBm results with $m \leq 8$. Thus, clearly the LSUB10 results will not fit with a leading-order extrapolation scheme of Eq. (45) with *any* value of the exponent ν, when used with the corresponding LSUBm results with lower values of m. By contrast, for values $\kappa \gtrsim 0.5$, the LSUB10 results fit well with the other LSUBm results in such an extrapolation. This effect is observed very clearly in Fig. 4(c) by a comparison of the two curves labelled LSUB∞(1) and LSUB∞(2), both of which are based on the extrapolation scheme of Eq. (45), but using the LSUBm results with $m = \{4, 6, 8\}$ and $m = \{4, 6, 8, 10\}$ respectively. The LSUB∞(1) result is particularly re-

vealing in that it produces a value of χ_d^{-1} which is flat and very close to zero (actually even slightly negative) over a range $0.36 \lesssim \kappa \lesssim 0.51$. When we also recall that the N-II(p) phase itself becomes unphysical (i.e., with $M < 0$) in the range $\kappa \lesssim 0.36$, this result is very suggestive indeed of SDVBC ordering becoming stable over the regime $\kappa_{c_2} < \kappa < \kappa_{c_3}$ where $\kappa_{c_3} \approx 0.51$. Interestingly, too, the portion of the corresponding LSUB∞(2) curve for χ_d^{-1} for values $\kappa \gtrsim 0.65$ agrees reasonably well with its LSUB∞(1) counterpart and also appears to be decreasing smoothly to zero at a similar value κ_{c_3}. Over the range $\kappa_{c_2} < \kappa < \kappa_{c_3}$ the fitted value for the exponent ν in Eq. (45) is very close to 1 for the LSUB∞(1) curve, while it varies much more over the range $2 \gtrsim \nu \gtrsim 1$ for the LSUB∞(2) curve. Both curves give a value for ν which smoothly approaches the value 2 as κ increases beyond κ_{c_3}.

The LSUB∞(ke) results obtained from using the extrapolation scheme of Eq. (44) also agree well with the LSUB∞(k) results from using Eq. (45) for values $\kappa \gtrsim 0.7$. Both the LSUB∞(1e) and LSUB∞(2e) fits yield a value $\nu \approx 2$ for the fitted exponent for values $\kappa \gtrsim 0.5$, the value of ν then drops sharply in both cases towards zero at the corresponding point where $\chi_d^{-1} \to 0$.

It is clear that extrapolating χ_d^{-1} is delicate in the range $\kappa \lesssim 0.65$. Nevertheless, from all of our results, taken together, it seems clear that there is a close competition between the N-II(p) and SDVBC phases as to which provides the stable GS phase for values $\kappa > \kappa_{c_2}$. When combined with our previous energy results, we have definite evidence that over the entire range $\kappa_{c_2} < \kappa < \kappa_{c_3}$ the stable GS phase has SDVBC ordering, probably mixed with N-II(p) ordering in all or part of that region; while for values $\kappa > \kappa_{c_3}$ the N-II(p) state alone provides the stable GS phase. A very precise value for κ_{c_3} is hard to predict on the basis of the present results, but our best estimate is $\kappa_{c_3} \approx 0.52(3)$.

V. SUMMARY AND DISCUSSION

In the range of values $0 \le \kappa \le 1$ for the frustration parameter $\kappa \equiv J_2/J_1$, we have found that the spin-$\frac{1}{2}$ J_1–J_2 isotropic XY model on the honeycomb lattice has four stable GS phases at $T = 0$. They exhibit, respectively, Néel ordering in the xy spin plane, Néel ordering in the z spin direction, SDVBC ordering, and Néel-II order in the xy spin plane, as illustrated in Fig. 5. For the corresponding isomorphic HC boson model the N(p) and N-II(p) phases with Néel and Néel-II forms of AFM ordering in the xy plane, which are both collinear spin-wave-type states, correspond to Bose-Einstein condensates (BECs) in which the lattice bosons are condensed, respectively, into momentum states with $\mathbf{Q} = \mathbf{\Gamma}$ and $\mathbf{Q} = \mathbf{M}^{*(l)}$; $l = 1, 2, 3$. Similarly, the N(z) state with Néel ordering along the z spin direction corresponds to a CDW state for the HC bosons.

The current spin-$\frac{1}{2}$ J_1–J_2 isotropic XY model of Eq. (2) exhibits both similarities and distinct differences in the structure of its GS phase diagram with that of its spin-$\frac{1}{2}$ Heisenberg counterpart of Eq. (1), by contrast with the classical ($s \to \infty$) versions of the models, which share exactly the same GS phase diagram. In both $s = \frac{1}{2}$ models quantum fluctuations serve to preserve the collinear AFM N(p) order (– but, of course, for the Heisenberg model all directions in spin space for the Néel ordering are equally likely –) out to larger values of κ than for the corresponding classical upper bound for Néel order of $\kappa_{\rm cl} = \frac{1}{6}$. Our CCM estimate for this first QCP at which N(p) order melts is $\kappa_{c_1} = 0.216(5)$ for the present XY model, which is very close to our earlier estimate of $\kappa_{c_1} = 0.207(3)$ for its spin-$\frac{1}{2}$ Heisenberg counterpart.[14] For the XY model our value for κ_{c_1} agrees extremely well with those of other recent calculations, including $\kappa_{c_1} = 0.210(8)$ from ED studies of various 24-site clusters,[40] and $\kappa_{c_1} \approx 0.22$ from a large-scale DMRG study on wide cylinders.[39] Both of these studies showed that the locations of the QCPs observed were relatively insensitive to finite-size effects. Of course, our own CCM results pertain to the thermodynamic ($N \to \infty$) limit, with no finite-size scaling required.

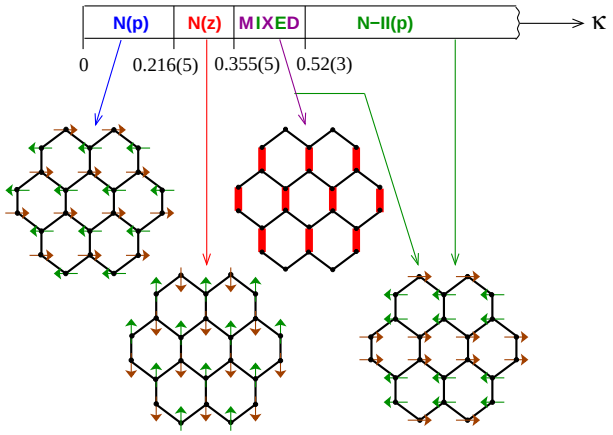

FIG. 5. (Color online) Phase diagram of the spin-1/2 J_1–J_2 isotropic XY model on the honeycomb lattice (with $J_1 > 0$ and $\kappa \equiv J_2/J_1 > 0$), as obtained by a CCM analysis. The quantum critical points are at $\kappa_{c_1} \approx 0.216(5)$, $\kappa_{c_2} \approx 0.355(5)$, and $\kappa_{c_3} \approx 0.52(3)$, as shown in the diagram. The MIXED state has SDVBC order over the whole range shown, which is probably mixed with N-II(p) ordering in all or part of the region.

Whereas, for the spin-$\frac{1}{2}$ Heisenberg model of Eq. (1) on the honeycomb lattice, our CCM study[14] showed that the Néel order that exists for $\kappa < \kappa_{c_1}$ gives way to PVBC order over a range $\kappa_{c_1} < \kappa < \kappa_{c_2}$, our present CCM study of its spin-$\frac{1}{2}$ XY counterpart has shown that the N(p) order gives way to N(z) order. In both models the transition at κ_{c_1} was found to be of continuous (second-order) type. Our current CCM estimate for the second QCP at which N(z) order melts in the XY model is $\kappa_{c_2} = 0.355(5)$, which may be compared with the corresponding second

QCP at $\kappa_{c_2} = 0.385(10)$ in the Heisenberg model at which the PVBC order melts. Once again, our value for κ_{c_2} for the XY model agrees very well with the corresponding estimates $\kappa_{c_2} = 0.356(9)$ from ED studies of various 24-site clusters[40] and $\kappa_{c_2} \approx 0.36$ from the aforementioned DMRG study.[39]

Despite the excellent agreement between the present CCM study and the DMRG[39] and ED[40] studies on the values of κ_{c_1} and κ_{c_2}, there is disagreement over the nature of the phase between these two QCPs. Thus, for example, whereas the DMRG study,[39] which was based on much larger clusters than is possible with available computational resources using the ED method, found clear evidence of N(z) ordering in this range, the ED study[40] concluded that the GS phase was a QSL state, after having specifically tested for other forms of ordering, including of the N(z) (or, equivalently, CDW) type, and found them to be absent in the largest (but still small) clusters studied. In view of our own and the DMRG studies it does seem likely that the absence of N(z) order in small clusters in the region $\kappa_{c_1} < \kappa < \kappa_{c_2}$ is a definite finite-size effect that does not pertain in the thermodynamic limit. Furthermore, it is clear from Fig. 3 that the order parameter M over the whole of the N(z) region is rather small, and that this form of order is relatively "fragile". Indeed, as a technical aside, it is this very fragility that makes solving the CCM LSUBm equations based on the N(z) model state considerably more computationally challenging, at a given level m of approximation, than those based on the other two model states.

We also note that a recent VMC study,[41] which used correlated variational QSL wave functions based on a decomposition of the underlying boson operators into a pair of spin-$\frac{1}{2}$ fermion (parton) operators, together with Gutzwiller projection to enforce the HC single-occupancy constraint and a long-range Jastrow factor, found that such QSL variational states do lie lower in energy than similar variational AFM spin-wave states based on N(p) or N-II(p) forms of order. However, although such variational AFM states have been shown to give reasonably accurate estimates for the GS energy for small clusters by comparison with ED results (and see, e.g., Table III of Ref. 55) in the N(p) regime, $\kappa < \kappa_{c_1}$, for example, those based on variational QSL states in the regime $\kappa_{c_1} < \kappa < \kappa_{c_2}$ have appreciable inaccuracies. Thus, for example, at $\kappa = 0.3$, the extrapolated VMC estimate for the GS energy per spin based on the QSL variational wave function is $E(\kappa = 0.3)/N = -0.28154(3)$ for the thermodynamic limit, $N \to \infty$ (see, e.g., Table III of the Supplemental Material of Ref. 41). Although this energy is lower than the comparable VMC estimates found that are based on either of the AFM [N(p) or N-II(p)] spin-wave trial states, it is still some 4.5% higher than our own extrapolated CCM result based on the N(z) model state.

It is difficult to intuit why N(z) order should appear in the XY spin model in the region $\kappa_{c_1} < \kappa < \kappa_{c_2}$, in the complete absence of any Ising-like pairwise interactions of the form $s_k^z s_l^z$. In the isomorphic HC boson model this phase manifests itself as a Mott insulator with one boson per two-site unit cell, and the N(z) order in the spin model translates to a CDW order that breaks the Z_2 sublattice (inversion) symmetry of the unit cell, in which the density $n_{\mathcal{A}}$ of bosons on sublattice $\mathcal{A}$ is higher than the density $n_{\mathcal{B}} = 1 - n_{\mathcal{A}}$ of bosons on sublattice $\mathcal{B}$. As we have seen, the maximum difference occurs at a value $\kappa \approx 0.279$ of the frustration parameter, where $n_{\mathcal{A}} \approx 0.642$ and $n_{\mathcal{B}} \approx 0.358$. Presumably for the HC boson model it is the HC constraint that somehow creates the LRO in fluctuations in the density operator in the presence of frustrated hopping, by the production of an induced NN density-density interaction.

Finally, just as in our earlier CCM study[15] of the spin-$\frac{1}{2}$ J_1–J_2 Heisenberg model of Eq. (1) on the honeycomb lattice, we find here for its spin-$\frac{1}{2}$ isotropic XY counterpart of Eq. (2) that for values $\kappa > \kappa_{c_2}$ there is a very close competition to form the stable GS phase between states with SDVBC and N-II(p) order. A similar finding was also reported in the DMRG study.[39] While the ED study[40] found that for $(1 >) \kappa > \kappa_{c_2}$ the small 24-spin clusters studied exhibited N-II(p) ordering, explicit examination of the dimer-dimer correlation function $D_{ij,kl} \equiv \langle (\mathbf{s}_i \cdot \mathbf{s}_j)(\mathbf{s}_k \cdot \mathbf{s}_l) \rangle$ and its associated structure factor, showed no evidence for dimer formation after appropriate finite-size scaling was performed. It seems clear, however, from our own results and those of others that the N-II(p) and SDVBC phases must lie very close in energy and these are unlikely to be easily resolved in calculations on finite clusters. Indeed in the DMRG study,[39] based on much larger (cylindrical) clusters than are feasible by ED, the stable GS phase at a given value $\kappa \approx 0.5$ depended on the shape and size of the cylinder. While on some cylindrical clusters the GS phase was the N-II(p) state, with the SDVBC state not even being metastable, on others the SDVBC pattern of dimer correlations was strongly indicated. From all of the available evidence it seems that only a method such as the CCM, in which one works from the outset in the thermodynamic limit ($N \to \infty$), might have sufficient accuracy to distinguish between the comparative stability of the SDVBC and N-II(p) phases. Our own best estimate is that the present spin-$\frac{1}{2}$ J_1–J_2 isotropic XY model on the honeycomb lattice has a third QCP at $\kappa_{c_3} \approx 0.52(3)$ such that for $\kappa_{c_2} < \kappa < \kappa_{c_3}$ the stable $T = 0$ GS phase has SDVBC order, but which is probably mixed with N-II(p) order over all or (the higher-κ) part of this range; while for $\kappa > \kappa_{c_3}$ it has N-II(p) order, at least for the range $\kappa < 1$ examined. Our earlier CCM analysis of the corresponding Heisenberg model of Eq. (1) on the honeycomb lattice[15] showed a similar QCP at a value $\kappa_{c_3} \approx 0.65(5)$.

Within the window $0 \leq \kappa \leq 1$ we have found no evidence for any kinds of ordering for the present spin-$\frac{1}{2}$ J_1–J_2 isotropic XY model on the honeycomb lattice other than the four forms shown in Fig. 5. Nevertheless, as $\kappa \to \infty$ the model of Eq. (2) reduces to a simple NN isotropic XY model on the two indepen-

dent triangular sublattices $\mathcal{A}$ and $\mathcal{B}$, for which the GS phase is known to have the 120° spin-wave ordering with $\mathbf{Q} = \mathbf{K}^{*(n)};\ n = 1, 2$. Although it is outside the scope of this study it might still be of interest to apply the CCM with model states of the classical spiral type discussed in Sec. II, to test whether for any range of values of κ in the region $\kappa > 1$ such quasiclassical spiral order is still stable under quantum fluctuations.

In this context we note that an ED study on 24-site clusters[40] found that the 120° ordering was established for all values $\kappa > 1.32(2)$, whereas the aforementioned VMC study of the same model[55] found some evidence for stability of both spiral order (of the type found in the classical version of the model for $\kappa > \frac{1}{2}$) in the range $1 \lesssim \kappa \lesssim 3.5$, and 120° order in the entire range $\kappa \gtrsim 3.5$. Nevertheless, it was clear from these investigations that the differences in energy between the states with spiral order and those with either N(p) or 120° order are very small in the region where spiral order is variationally preferred among the class of trial wave functions examined. It thus remains an interesting open question as to whether spiral order remains stable for the spin-$\frac{1}{2}$ J_1–J_2 isotropic XY model on the honeycomb lattice in the thermodynamic limit ($N \to \infty$) for any range of values of κ, or whether a further direct transition occurs at a higher QCP ($\kappa_{c_4} > 1$), between phases with N(p) order (with $\mathbf{Q} = \mathbf{M}^{*(l)};\ l = 1, 2, 3$) and 120° order (with $\mathbf{Q} = \mathbf{K}^{*(n)};\ n = 1, 2$).

Finally, we note that in view of the differences in the $T = 0$ GS phase diagrams of the two related spin-$\frac{1}{2}$ J_1–J_2 models of Eqs. (1) and (2) on the honeycomb lattice, it might also be of interest to investigate models that interpolate between them. One simple way to do this would be to replace both the NN and NNN isotropic interactions by XXZ-type interactions. In the language of the isomorphic HC boson model of Eq. (20) this would be equivalent to the addition of off-site Ising-like two-body interaction terms proportional to $n_k n_l$ between NN and NNN pairs. Such a HC Bose-Hubbard-Haldane type of model has been studied recently[56] by ED of clusters containing up to 30 lattice sites, but with an effective XXZ interaction only between NN sites (i.e., with the effective NNN interactions still of the isotropic XY type). An interesting related study of a spin-$\frac{1}{2}$ J_1–J_2–J_3 model on the honeycomb lattice,[57] in which third-nearest-neighbor exchange couplings are also included, has also been performed recently. It incorporated XXZ interactions on all three bonds, but only examined the case of ferromagnetic quantum fluctuations in order to avoid the minus-sign problem in the QMC simulations. Although, as we have indicated in Sec. III, the sign can be eliminated by a sublattice rotation for the J_1 and J_3 interactions, this cannot be done for the J_2 interactions, and hence those results have little direct relevance to the present case, especially since the J_1–J_2–J_3 model was only studied for the special case when $J_3 = J_2$.

ACKNOWLEDGMENTS

We thank the University of Minnesota Supercomputing Institute for the grant of supercomputing facilities for this research.

[1] E. Rastelli, A. Tassi, and L. Reatto, Physica B & C **97**, 1 (1979).
[2] J. B. Fouet, P. Sindzingre, and C. Lhuillier, Eur. Phys. J. B **20**, 241 (2001).
[3] A. Mulder, R. Ganesh, L. Capriotti, and A. Paramekanti, Phys. Rev. B **81**, 214419 (2010).
[4] D. C. Cabra, C. A. Lamas, and H. D. Rosales, Phys. Rev. B **83**, 094506 (2011).
[5] R. Ganesh, D. N. Sheng, Y.-J. Kim, and A. Paramekanti, Phys. Rev. B **83**, 144414 (2011).
[6] B. K. Clark, D. A. Abanin, and S. L. Sondhi, Phys. Rev. Lett. **107**, 087204 (2011).
[7] D. J. J. Farnell, R. F. Bishop, P. H. Y. Li, J. Richter, and C. E. Campbell, Phys. Rev. B **84**, 012403 (2011).
[8] A. F. Albuquerque, D. Schwandt, B. Hetényi, S. Capponi, M. Mambrini, and A. M. Läuchli, Phys. Rev. B **84**, 024406 (2011).
[9] H. Mosadeq, F. Shahbazi, and S. A. Jafari, J. Phys.: Condens. Matter **23**, 226006 (2011).
[10] J. Oitmaa and R. R. P. Singh, Phys. Rev. B **84**, 094424 (2011).
[11] F. Mezzacapo and M. Boninsegni, Phys. Rev. B **85**, 060402(R) (2012).
[12] P. H. Y. Li, R. F. Bishop, D. J. J. Farnell, J. Richter, and C. E. Campbell, Phys. Rev. B **85**, 085115 (2012).
[13] R. F. Bishop and P. H. Y. Li, Phys. Rev. B **85**, 155135 (2012).
[14] R. F. Bishop, P. H. Y. Li, D. J. J. Farnell, and C. E. Campbell, J. Phys.: Condens. Matter **24**, 236002 (2012).
[15] R. F. Bishop, P. H. Y. Li, and C. E. Campbell, J. Phys.: Condens. Matter **25**, 306002 (2013).
[16] J. Villain, J. Phys. (France) **38**, 385 (1977).
[17] J. Villain, R. Bidaux, J. P. Carton, and R. Conte, J. Phys. (France) **41**, 1263 (1980).
[18] R. F. Bishop, J. B. Parkinson, and Y. Xian, Phys. Rev. B **44**, 9425 (1991).
[19] C. Zeng, D. J. J. Farnell, and R. F. Bishop, J. Stat. Phys. **90**, 327 (1998).
[20] S. E. Krüger, J. Richter, J. Schulenburg, D. J. J. Farnell, and R. F. Bishop, Phys. Rev. B **61**, 14607 (2000).
[21] R. F. Bishop, D. J. J. Farnell, S. E. Krüger, J. B. Parkinson, J. Richter, and C. Zeng, J. Phys.: Condens. Matter **12**, 6887 (2000).
[22] D. J. J. Farnell, R. F. Bishop, and K. A. Gernoth, Phys. Rev. B **63**, 220402(R) (2001).
[23] R. Darradi, J. Richter, and D. J. J. Farnell, Phys. Rev. B **72**, 104425 (2005).

[24] D. Schmalfuß, R. Darradi, J. Richter, J. Schulenburg, and D. Ihle, Phys. Rev. Lett. **97**, 157201 (2006).
[25] R. F. Bishop, P. H. Y. Li, R. Darradi, J. Schulenburg, and J. Richter, Phys. Rev. B **78**, 054412 (2008).
[26] R. F. Bishop, P. H. Y. Li, R. Darradi, and J. Richter, J. Phys.: Condens. Matter **20**, 255251 (2008).
[27] R. Darradi, O. Derzhko, R. Zinke, J. Schulenburg, S. E. Krüger, and J. Richter, Phys. Rev. B **78**, 214415 (2008).
[28] R. F. Bishop, P. H. Y. Li, D. J. J. Farnell, and C. E. Campbell, Phys. Rev. B **79**, 174405 (2009).
[29] J. Richter, R. Darradi, J. Schulenburg, D. J. J. Farnell, and H. Rosner, Phys. Rev. B **81**, 174429 (2010).
[30] R. F. Bishop, P. H. Y. Li, D. J. J. Farnell, and C. E. Campbell, Phys. Rev. B **82**, 024416 (2010).
[31] R. F. Bishop, P. H. Y. Li, D. J. J. Farnell, and C. E. Campbell, Phys. Rev. B **82**, 104406 (2010).
[32] J. Reuther, P. Wölfle, R. Darradi, W. Brenig, M. Arlego, and J. Richter, Phys. Rev. B **83**, 064416 (2011).
[33] O. Götze, D. J. J. Farnell, R. F. Bishop, P. H. Y. Li, and J. Richter, Phys. Rev. B **84**, 224428 (2011).
[34] R. F. Bishop, P. H. Y. Li, D. J. J. Farnell, J. Richter, and C. E. Campbell, Phys. Rev. B **85**, 205122 (2012).
[35] P. H. Y. Li, R. F. Bishop, D. J. J. Farnell, and C. E. Campbell, Phys. Rev. B **86**, 144404 (2012).
[36] P. H. Y. Li, R. F. Bishop, C. E. Campbell, D. J. J. Farnell, O. Götze, and J. Richter, Phys. Rev. B **86**, 214403 (2012).
[37] P. H. Y. Li, R. F. Bishop, and C. E. Campbell, Phys. Rev. B **88**, 144423 (2013).
[38] R. F. Bishop, P. H. Y. Li, and C. E. Campbell, Phys. Rev. B **88**, 214418 (2013).
[39] Z. Zhu, D. A. Huse, and S. R. White, Phys. Rev. Lett. **111**, 257201 (2013).
[40] C. N. Varney, K. Sun, V. Galitski, and M. Rigol, Phys. Rev. Lett. **107**, 077201 (2011).
[41] J. Carrasquilla, A. D. Ciolo, F. Becca, V. Galitski, and M. Rigol, Phys. Rev. B **88**, 241109(R) (2013).
[42] T. Matsubara and H. Matsuda, Prog. Theor. Phys. **16**, 569 (1956).
[43] J. Voit, Phys. Rev. B **45**, 4027 (1992).
[44] M. Nakamura, J. Phys. Soc. Jpn. **68**, 3123 (1999).
[45] M. Nakamura, Phys. Rev. B **61**, 16377 (2000).
[46] F. D. M. Haldane, Phys. Rev. Lett. **61**, 2015 (1988).
[47] R. F. Bishop and H. G. Kümmel, Phys. Today **40(3)**, 52 (1987).
[48] J. S. Arponen and R. F. Bishop, Ann. Phys. (N.Y.) **207**, 171 (1991).
[49] R. F. Bishop, Theor. Chim. Acta **80**, 95 (1991).
[50] R. F. Bishop, in *Microscopic Quantum Many-Body Theories and Their Applications*, Lecture Notes in Physics Vol. 510, edited by J. Navarro and A. Polls (Springer-Verlag, Berlin, 1998) p. 1.
[51] D. J. J. Farnell and R. F. Bishop, in *Quantum Magnetism*, Lecture Notes in Physics Vol. 645, edited by U. Schollwöck, J. Richter, D. J. J. Farnell, and R. F. Bishop (Springer-Verlag, Berlin, 2004) p. 307.
[52] R. Darradi, J. Richter, J. Schulenburg, R. F. Bishop, and P. H. Y. Li, J. Phys.: Conf. Ser. **145**, 012049 (2009).
[53] We use the program package CCCM of D. J. J. Farnell and J. Schulenburg, see http://www-e.uni-magdeburg.de/jschulen/ccm/index.html.
[54] J. Oitmaa, C. J. Hamer, and Z. Weihong, Phys. Rev. B **45**, 9834 (1992).
[55] A. D. Ciolo, J. Carrasquilla, F. Becca, M. Rigol, and V. Galitski, Phys. Rev. B **89**, 094413 (2014).
[56] C. N. Varney, K. Sun, V. Galitski, and M. Rigol, New J. Phys. **14**, 115028 (2012).
[57] A. Kalz, M. Arlego, D. Cabra, A. Honecker, and G. Rossini, Phys. Rev. B **85**, 104505 (2012).